

1 **Title:** Roles of cellular NSF protein in entry and nuclear egress of budded  
2 virions of *Autographa californica* multiple nucleopolyhedrovirus

3

4 Ya Guo<sup>1</sup>, Qi Yue<sup>1</sup>, Jinli Gao<sup>1</sup>, Zhe Wang<sup>1</sup>, Yun-Ru Chen<sup>2#</sup>, Gary W. Blissard<sup>2</sup>,  
5 Tong-Xian Liu<sup>\*1</sup>, and Zhaofei Li<sup>\*1</sup>

6

7 <sup>1</sup>State Key Laboratory of Crop Stress Biology for Arid Areas, Key Laboratory of  
8 Northwest Loess Plateau Crop Pest Management of Ministry of Agriculture,  
9 College of Plant Protection, Northwest A&F University, Yangling, Shaanxi  
10 712100, China

11 <sup>2</sup>Boyce Thompson Institute, Cornell University, Ithaca, New York 14853

12 #Present address: State Key Laboratory of Agrobiotechnology, School of Life  
13 Science, The Chinese University of Hong Kong, Shatin, NT, Hong Kong, China  
14

15 Running Title: Requirement for NSF in baculovirus entry and egress

16 Keywords: SNARE, NSF, baculovirus, AcMNPV, virus entry and egress

17 Word count: Abstract, 232 words; Text, 10385 words.

18

19 \*Corresponding authors

20 Zhaofei Li, Tong-Xian Liu

21 College of Plant Protection, Northwest A&F University,

22 Taicheng Road, Yangling, Shaanxi, China, 712100

23 Email: [zhaofeili73@outlook.com](mailto:zhaofeili73@outlook.com), [txliu@nwsuaf.edu.cn](mailto:txliu@nwsuaf.edu.cn)

24 Tel: 86-18792598371 (ZL), 86-13709141817 (TXL)

25 **Abstract**

26 In eukaryotic cells, the soluble N-ethylmaleimide-sensitive factor (NSF)  
27 attachment protein receptor (SNARE) proteins comprise the minimal  
28 machinery that triggers fusion of transport vesicles with their target  
29 membranes. Comparative studies revealed that genes encoding the  
30 components of the SNARE system are highly conserved in yeast, insect, and  
31 human genomes. Upon infection of insect cells by the virus AcMNPV, the  
32 transcript levels of most SNARE genes were initially up-regulated. We found  
33 that overexpression of dominant-negative (DN) forms of NSF or knock-down of  
34 the expression of NSF, the key regulator of the SNARE system, significantly  
35 affected the infectious AcMNPV production. In cells expressing DN NSF,  
36 entering virions were trapped in the cytoplasm or transported to the nucleus  
37 with low efficiency. The presence of DN NSF also moderately reduced  
38 trafficking of the viral envelope glycoprotein GP64 to the plasma membrane  
39 but dramatically inhibited production of infectious BV. TEM analysis of  
40 infections in cells expressing DN NSF revealed that progeny nucleocapsids  
41 were retained in a perinuclear space surrounded by inner and outer nuclear  
42 membranes. Several baculovirus conserved (core) proteins (Ac76, Ac78,  
43 GP41, Ac93, and Ac103) that are important for infectious budded virion  
44 production, were found to associate with NSF, and NSF was detected within  
45 the assembled BV. Together, these data indicate that the cellular SNARE  
46 system is involved in AcMNPV infection and that NSF is required for efficient  
47 entry and nuclear egress of budded virions of AcMNPV.

48 **Importance**

49 Little is known regarding the complex interplay between cellular factors and  
50 baculoviruses during viral entry and egress. Here we examined the cellular  
51 SNARE system, which mediates the fusion of vesicles in healthy cells, and its  
52 relation to baculovirus infection. Using a dominant negative (DN) approach and  
53 an RNAi knockdown, we demonstrated that a general disruption of the SNARE  
54 machinery significantly inhibited the production of infectious budded virions  
55 (BV) of AcMNPV. The presence of a DN NSF protein resulted in low efficiency  
56 entry of BV and the retention of progeny nucleocapsids in the perinuclear  
57 space during egress. Combined with these effects, we also found that several  
58 conserved (core) baculovirus proteins closely associate with NSF, and these  
59 results suggest their involvement in the egress of BV. Our findings are the first  
60 to demonstrate that the SNARE system is required for efficient entry of BV and  
61 nuclear egress of progeny nucleocapsids of baculoviruses.

## 62 Introduction

63 In eukaryotic cells, soluble N-ethylmaleimide-sensitive factor attachment  
64 protein receptor (SNARE) proteins constitute the minimal machinery that  
65 mediates the fusion of transport vesicles with target membranes (1, 2). These  
66 evolutionarily conserved SNARE proteins constitute a large family of  
67 approximately 50 or more proteins in mammals and are classified as either  
68 v-SNAREs (found on vesicle membranes) or t-SNAREs (found on target  
69 membranes) (1). During the membrane fusion process, a highly stable  
70 four-helix bundle is formed from an interaction of the v-SNARE and t-SNARE  
71 proteins that are anchored in opposing membranes. Most v-SNARE and  
72 t-SNARE protein encodes a 50-60 amino acid SNARE motif, a motif that  
73 contains a heptad repeat that forms a coiled coil structure. Four SNARE  
74 proteins called SNAP-23 (synaptosome-associated protein of 23 kDa),  
75 SNAP-25, SNAP-29, and SNAP-47, each contain two tandem SNARE motifs  
76 separated by a linker region. The coiled coil structures from each of four v-  
77 SNAREs and four t-SNAREs interact to form the four-helix bundle during  
78 fusion. The center of the four-helix bundle contains 16 stacked layers of  
79 interacting side chains, which are largely hydrophobic, except for a central "0"  
80 layer that contains three highly conserved glutamine (Q) residues and one  
81 highly conserved arginine (R) residue, each contributed by one of the subunit  
82 proteins (see Figure 2 in reference (1)). Based on these conserved residues  
83 and the similarity of SNARE motifs, SNARE proteins are classified into four  
84 main types: Qa- (SNAREs containing a SNARE motif that is close to that of  
85 syntaxin 1, 2, 3, 4, 5, 7, 11, 13, 16, 17 or 18), Qb- (SNAREs containing a  
86 SNARE motif that is similar to the N-terminal SNARE motif of SNAP-25), Qc-

87 (SNAREs containing a SNARE motif that is similar to the C-terminal SNARE  
88 motif of SNAP-25) and R-SNAREs (SNAREs containing a SNARE motif that is  
89 close to that of vesicle-associated membrane protein (VAMP) proteins).  
90 Functional SNARE complexes that drive membrane fusion need one of each of  
91 the above four SNARE types (1, 3). These four main types of SNARE proteins  
92 can be further classified into 20 different conserved groups which participate in  
93 diverse intracellular trafficking processes (4). At a late step of membrane  
94 fusion, SNARE complexes are disassembled into individual SNARE proteins  
95 for recycling (1). This disassembly process is catalyzed by a protein called  
96 N-ethylmaleimide-sensitive factor (NSF) and its adaptor protein,  $\alpha$ -soluble NSF  
97 attachment protein ( $\alpha$ -SNAP) (5-7). NSF is an ATPase that belongs to the  
98 AAA+ ATPase family, a family of proteins that are involved in a variety of  
99 cellular activities (8). NSF functions as a homohexamer and each subunit  
100 consists of the N-terminal domain (NSF-N) and two AAA+ domains (NSF-D1  
101 and NSF-D2). The N domain is required for interaction with the  
102  $\alpha$ -SNAP-SNARE complex. The D1 domain provides ATPase activity  
103 associated with SNARE disassembly, and the D2 domain is involved in  
104 nucleotide-dependent hexamerization (9-11). Two well-characterized  
105 mutations of NSF (NSF<sup>E329Q</sup> and NSF<sup>R385A</sup>) result in failure of NSF to bind or  
106 hydrolyze ATP. Inactivation of NSF function by overexpressing these  
107 dominant-negative (DN) forms of NSF leads to failure in disassembly of  
108 SNARE complexes and consequent disruption of SNARE function (10, 12, 13).

109 A number of studies have demonstrated an important role of the cellular  
110 SNARE machinery in the replication of certain mammalian viruses. In human  
111 cytomegalovirus (HCMV) infected cells, SNARE protein SNAP-23 is found in

112 the region of viral assembly in the cytoplasm., and depletion of SNAP-23 by  
113 RNA interference significantly reduced infectious HCMV production and  
114 disrupted virion assembly or maturation (14). For another herpesvirus, human  
115 herpes virus 6 (HHV-6), viral glycoproteins M and N (gM/gN) interact with  
116 VAMP3, a SNARE involved in vesicular transport. During the late phase of  
117 virus infection, the expression level of VAMP3 was significantly up-regulated  
118 and VAMP3 becomes incorporated into mature HHV-6 virions (15). The  
119 interaction of a viral protein with host SNARE system components was also  
120 reported in cells infected with human parainfluenza virus type 3 (HPIV3). The  
121 HPIV3 phosphoprotein (P) interacts with SNAP-29, and through this interaction,  
122 HPIV3 induces incomplete autophagy by inhibiting the interaction of SNAP-29  
123 with syntaxin 17 (Syx17), a SNARE associated with autophagosome-lysosome  
124 fusion (16). Additionally, down-regulation of Syx17 and impairment of  
125 autophagosome-lysosome fusion by hepatitis C virus (HCV) are critical for  
126 HCV release (17). In another example of the requirement for SNARE protein  
127 functions in viral infections, it was found that overexpression of  
128 dominant-negative (DN) NSF (NSF<sup>E329Q</sup>) substantially reduced production of  
129 infectious human immunodeficiency virus (HIV-1) and this results from reduced  
130 levels of Gag at the plasma membrane (18, 19). In addition to the role of  
131 SNARE proteins in efficient assembly or egress of viruses, SNARE proteins  
132 are also involved in viral entry in many cases. Inhibition of VAMP8 (a SNARE  
133 protein that participates in endosomal fusion) significantly decreases influenza  
134 A virus and vesicular stomatitis virus (VSV) entry into host cells (20).  
135 Inactivation of VAMP3 also results in defects in bunyavirus (Uukuniemi virus)  
136 entry (21).

137 Baculoviruses represent a family of large double-stranded DNA viruses  
138 with circular genomes that range from 80 to 180 kb. Many baculoviruses are  
139 highly pathogenic to their insect hosts (22). These viruses are widely used as  
140 biological insecticides, protein expression vectors, and mammalian cell  
141 transduction vectors (23-25). During the infection cycle, baculoviruses produce  
142 two types of virions: occlusion-derived virions (ODV) and budded virions (BV).  
143 ODV and BV are identical in genomic DNA content and nucleocapsid structure.  
144 However, they differ in the source and composition of their envelopes and in  
145 their functional roles in the infection cycle in the animal. ODV are acquired  
146 orally and initiate the primary infection in the midgut epithelium. Within midgut  
147 epithelial cells, BV is produced by budding from the cell surface. BV spread the  
148 viral infection from cell to cell within the infected insect. BV obtain the virion  
149 envelope from the plasma membrane, whereas ODV assemble in the nucleus  
150 and acquire their envelopes from virus-induced intranuclear microvesicles,  
151 which are derived from the inner nuclear membrane (22). *Autographa*  
152 *californica multiple nucleopolyhedrovirus* (AcMNPV) is the best-studied  
153 baculovirus and is the type species of the *Baculoviridae*. BV of AcMNPV enter  
154 host cells via clathrin-mediated endocytosis (26). The major viral envelope  
155 glycoprotein, GP64, is essential for receptor binding and low-pH triggered  
156 membrane fusion (27). During entry, the acidification of endosomes triggers a  
157 conformational change in GP64, which then mediates fusion of the viral  
158 envelope and endosomal membranes, releasing the nucleocapsid into the  
159 cytosol (28). Nucleocapsids are then transported to the nuclear periphery via  
160 actin-based motility (29), and enter the nucleus through the nuclear pore  
161 complex (22, 30). After the viral genome is released within the nucleus, viral

162 transcription and DNA replication occur and are subsequently followed by  
163 progeny nucleocapsid assembly in a dense region referred to as the virogenic  
164 stroma (VS) (22). Some progeny nucleocapsids exit the nucleus. During this  
165 egress from the nucleus, nucleocapsids appear to acquire an envelope by  
166 blebbing of the nuclear membranes (31). This double envelope (derived  
167 presumably from inner and outer nuclear membranes) appears to be lost in the  
168 cytosol as naked nucleocapsids are frequently observed in the cytosol and in  
169 the process of budding at the plasma membrane (22, 31). Because enveloped  
170 virions found within the cytosol represent a virus-induced vesicle, the loss of  
171 the double envelope within the cytosol may involve a fusion process that could  
172 be mediated by the cellular SNARE system. Intriguingly, several host proteins  
173 involved in vesicular transport have been identified in purified budded virions of  
174 AcMNPV by mass spectrometry (32).

175 To investigate whether the host cellular SNARE machinery is required for  
176 AcMNPV infection, we first analyzed the transcript levels of the SNARE genes  
177 in AcMNPV-infected insect cells (33) and found that most of the SNARE  
178 transcripts were up-regulated upon AcMNPV infection. We cloned the NSF  
179 gene from Sf9 cells, generated dominant-negative forms of Sf9 NSF, and  
180 analyzed the effects of DN NSF proteins on AcMNPV BV entry, viral replication,  
181 and BV egress. Our results demonstrated that NSF is required for efficient  
182 entry of AcMNPV BV into Sf9 cells, and for egress of BV. In addition, we found  
183 that NSF associates with several conserved (core) viral proteins suggesting  
184 that NSF associations with viral proteins may be involved in egress or  
185 assembly of AcMNPV BV.



186 **Materials and methods**

187 **Annotation of insect SNARE genes**

188 SNARE genes of the yeast *Saccharomyces cerevisiae* and the orthologs  
189 from the human genome were used for searches of insect genomes using  
190 BLASTP and TBLASTN programs. BLAST searches were performed using  
191 databases of sequenced insect genomes from 6 Orders, including Coleoptera  
192 (*Tribolium castaneum*; <http://beetlebase.org>), Diptera (*Drosophila*  
193 *melanogaster*, *Aedes aegypti*, *Anopheles gambiae*, and *Culex*  
194 *quinquefasciatus*; <http://flybase.org> and <http://www.vectorbase.org>), Hemiptera  
195 (*Acyrtosiphon pisum*; <http://www.aphidbase.com>), Hymenoptera (*Apis*  
196 *mellifera*, *Nasonia vitripennis*, and *Harpegnathos saltator*,  
197 <http://hymenopteragenome.org>), Lepidoptera (*Bombyx mori* and *Danaus*  
198 *plexippus*; <http://silkworm.genomics.org.cn> and  
199 <http://monarchbase.umassmed.edu>), and Phthiraptera (*Pediculus humanus*  
200 *corporis*; <http://www.vectorbase.org>). Specific BLAST searches were also  
201 carried out at the National Center for Biotechnology Information (NCBI).

202 **Cells, transfections, and infections**

203 *Spodoptera frugiperda* Sf9, *Trichoplusia ni* Tn5B1-4 (High 5) and Sf9<sup>Op1D</sup> (a  
204 cell line stably expressing *Orgyia pseudotsugata* (Op)MNPV GP64 (34)) cells  
205 were cultured at 27° in TNMFH medium (Sigma-Aldrich) containing 10% fetal  
206 bovine serum (FBS, Gibco). The cells in 6-well plates (1×10<sup>6</sup> cells per well) or  
207 12-well plates (2×10<sup>5</sup> cells per well) were transfected with plasmid or bacmid  
208 DNA or double-strand (ds)-RNA using a CaPO<sub>4</sub> precipitation method (28). For  
209 virus infections, virus inoculum was added to cells and incubated for 1 h. The  
210 cells were washed once in TNMFH. Times postinfection (p.i.) were calculated

211 from the time the viral inoculum was added.

## 212 **NSF cDNA cloning**

213 Total RNA was extracted from Sf9 cells by using an RNAiso plus kit  
214 (TaKaRa). The first-strand DNA complementary to the mRNA (cDNA) was  
215 synthesized by using AMV reverse transcriptase and an oligo-dT primer  
216 according to the manufacturer's instructions (TaKaRa). Gene-specific primers  
217 SfNsfF and SFNsfR, and NsfF and NsfR (Table 1), targeted to the Sf9 NSF  
218 ORF and the C-terminus of Sf9 NSF ORF, were designed based on the EST  
219 sequences at SPODOBASE database (<http://bioweb.ensam.inra.fr/spodobase>)  
220 (35). The PCR-amplified NSF ORF and a 90 bp fragment of NSF products  
221 were separately cloned into pMD18-T vector (TaKaRa) and sequenced with  
222 M13-47, M13-48, and NSF-specific primers. The pMD18-T vector containing  
223 the ORF of NSF and the small fragment of NSF was designated as  
224 NSFpMD18 and NSF90pMD18.

## 225 **Analysis of the transcription of NSF**

226 Sf9 cells in 6-well plates ( $1 \times 10^6$  cells per well) were infected with wild-type  
227 AcMNPV at an MOI of 10. At 1, 3, 6, 12, 18, 24, 36, and 48 h p.i., the infected  
228 and uninfected cells were collected and total RNA was extracted by using an  
229 RNAiso plus kit (TaKaRa). The genomic DNA elimination and first-strand DNA  
230 complementary to mRNA (cDNA) synthesis were performed with  
231 PrimeScript<sup>TM</sup> RT reagent kit with gDNA eraser and an oligo-dT primer  
232 (TaKaRa). The transcript of NSF was quantified by real-time PCR (IQ<sup>TM</sup>5  
233 Multicolor Real-Time PCR Detection System, Bio-Rad). Each PCR mixture  
234 contained 5  $\mu$ l SYBR<sup>®</sup> Premix ExTaq II (TaKaRa), 1.25  $\mu$ M each primer, and  
235 500 pg of the cDNA template. Primers NsfF: 5'-

236 ACCGCCTTAGCCGCTGAACT-3' and NsfR: 5'-  
237 AGACTCCGTGAATCCGACCATGT-3' were used to amplify a fragment of 90  
238 bp of Sf9 NSF. Thermal cycling conditions were one cycle of 95° for 3min,  
239 followed by 40 cycles of 95° for 10s, and 60° for 45s. A standard curve was  
240 generated by a serial dilution of NSF90pMD18. The transcript levels of NSF  
241 were expressed as numbers of transcript copies per cell.

#### 242 **Mutagenesis and construction of plasmids, bacmids, and viruses**

243 PCR primers and the plasmid constructs are listed in Table 1 and Table 2,  
244 respectively. The ORF of NSF containing a translation stop codon mutation  
245 (TAA to TAC) was generated by PCR using NSFpMD18 as the template and  
246 primers SfNsfXF and SfNsfER, which contain XbaI and EcoRI sites,  
247 respectively. The PCR product was digested with XbaI and EcoRI and inserted  
248 into the plasmid Vps4-GFPpBlue (36) under the control of the AcMNPV *ie1*  
249 immediately early/late promoter to replace Vps4 and yield the C-terminal  
250 GFP-tagged NSF transient expression plasmid NSF-GFPpBlue. Two point  
251 mutations, E329Q and R385A, were separately introduced into NSF by overlap  
252 PCR using NSFpMD18 as a template and primers NsfE329QF, NsfE329QR,  
253 NsfR385AF, and NsfR385AR. The PCR products were digested with XbaI and  
254 EcoRI and cloned into the plasmid Vps4-GFPpBlue to replace Vps4 and yield  
255 NSF<sup>E329Q</sup>-GFPpBlue and NSF<sup>R385A</sup>-GFPpBlue. All of the plasmids were  
256 confirmed by restriction enzyme analysis and DNA sequencing. The previously  
257 constructed gfppBlue (36) was used as a GFP-expressing control plasmid.

258 To construct a bimolecular fluorescent complementation (BiFC) system, the  
259 ORF of mCherry was separated as two fragments between amino acid  
260 positions 159 and 160 as described previously (37). A backbone expression

261 plasmid pIE was generated by inserting a multiple cloning site (MCS,  
262 5'TCTAGAATGGGATCCACTAGTCCGCGGCCCGGGCTGCAGGATATCGAA  
263 TTC3') into the XbaI and EcoRI sites of pBiepA (38) to replace the ORF of  
264 GP64. The N- and C-terminal fragments of mCherry (designated as Nm and  
265 Cm) containing the linker sequence GTSGGSG and the HA or c-Myc epitope  
266 tag were amplified by PCR using mCherryGUS bacmid DNA (36) as template  
267 and inserted into the XbaI and BamHI, or the XbaI and EcoRI sites of pIE to  
268 generate the BiFC expression plasmids Nm-HApBlue, HA-NmpBlue,  
269 Cm-MycpBue, or Myc-CmpBlue (Table 2). The immunoprecipitation vectors  
270 pIE-HA-MCS, pIE-Myc-MCS, pIE-MCS-HA, and pIE-MCS-Myc, which contain  
271 the HA or c-Myc epitope tag, were constructed in a similar manner (Table 2).  
272 The NSF coding region, obtained by digesting NSF-GFPpBlue with XbaI and  
273 EcoRI, was inserted into the MCS sites of the BiFC and immunoprecipitation  
274 vectors. AcMNPV genes (*ac11*, *ac76*, *ac78*, *ac80 (gp41)*, *ac93*, *ac103*, *ac142*,  
275 *ac146*, *lef3*) were amplified by PCR and digested with XbaI and EcoRI or  
276 BamHI and EcoRI, and then the coding region of each viral gene was also  
277 inserted into the MCS sites of the vectors as described above (Table 2). All of  
278 the plasmids were confirmed by DNA sequencing.

279 Recombinant AcMNPV bacmids expressing GFP, GFP-tagged NSF (WT or  
280 with mutations), and c-Myc tagged NSF were constructed by inserting a  
281 cassette containing GFP, NSF-GFP, NSF<sup>E329Q</sup>-GFP, NSF<sup>R385A</sup>-GFP, or  
282 NSF-Myc under the control of the AcMNPV *ie1* promoter, into a pFastbac  
283 plasmid (GUSpFB) that contains a  $\beta$ -glucuronidase (GUS) gene under the  
284 control of the AcMNPV *p6.9* late promoter. The resulting pFastbac constructs  
285 were each inserted into the polyhedrin locus of an AcMNPV bacmid

286 (bMON14272) by Tn7-mediated transposition (39). The resulting recombinant  
287 bacmids were separately named GFPBac, NSF-GFPBac, NSF<sup>E329Q</sup>-GFPBac,  
288 NSF<sup>R385A</sup>-GFPBac, and NSF-MycBac. All constructs were verified by DNA  
289 sequencing. The *gp64* knockout AcMNPV bacmids, LacZGUS-*gp64*<sup>ko</sup> and  
290 mCherryGUS-*gp64*<sup>ko</sup>, were constructed as described earlier (36). Plasmids  
291 and bacmids were purified using a Midiprep kit (Invitrogen). The *gp64*  
292 knockout viruses, LacZGUS-*gp64*<sup>ko</sup> and mCherryGUS-*gp64*<sup>ko</sup>, were grown and  
293 titered in Sf9<sup>OP1D</sup> cells that constitutively express OpMNPV GP64 (34).  
294 Wild-type AcMNPV encoding VP39-triple mCherry (AcMNPV-3mC) (29) was  
295 kindly provided by Taro Ohkawa and Matthew Welch (University of California,  
296 Berkeley).

### 297 **Cell viability assay**

298 Cell viability, upon overexpression of NSF or the NSF DN constructs  
299 NSF<sup>E329Q</sup> and NSF<sup>R385A</sup>, was assessed using the CellTiter96<sup>®</sup> AQueous One  
300 Solution Cell Proliferation Assay (MTS, Promega) according to the  
301 manufacturer's recommendations. Briefly, Sf9 cells in 6-well plates were  
302 transfected with 3  $\mu$ g of the plasmid expressing GFP, NSF-GFP, NSF<sup>E329Q</sup>-GFP,  
303 or NSF<sup>R385A</sup>-GFP. At 12, 24, and 36 h posttransfection (p.t.), the cells were  
304 incubated with CellTiter 96<sup>®</sup> AQueous One Solution reagent for 2 h at 27° and  
305 absorbance at 490 nm was monitored using a 96-well plate reader (Tecan  
306 iControl Reader, Mannedorf, Switzerland).

### 307 **Infectivity complementation assay**

308 Sf9 and High 5 cells in 6-well plates were co-transfected with 3  $\mu$ g of  
309 pBieGP64 (38) expressing GP64 and 3  $\mu$ g of a plasmid expressing GFP,  
310 NSF-GFP, NSF<sup>E329Q</sup>-GFP, or NSF<sup>R385A</sup>-GFP (Typically, we observed that about

311 70-80% cells showed GFP signals at 24 h post-transfection). At 12 h p.t., cells  
312 were infected with the GP64 knockout virus mCherryGUS-*gp64*<sup>ko</sup> at a  
313 multiplicity of infection (MOI) of 1 or 5. At 24 h p.i., the supernatants and cells  
314 were separately collected and virus titers were measured by 50% tissue  
315 culture infectious dose (TCID<sub>50</sub>) assays on Sf9<sup>OP1D</sup> cells. Cell samples were  
316 analyzed for the expression of GP64, NSF and its DN mutants by Western  
317 blotting.

### 318 **RNAi assay**

319 The dsRNA-based RNA interference (RNAi) assay was performed as  
320 described previously (40) with modifications. A 315 bp or 495 bp fragment of  
321 the coding sequence of Sf9 NSF or GFP was amplified by PCR. The PCR  
322 primers were designed with the SnapDragon tool  
323 ([http://www.flyrnai.org/cgi-bin/RNAi\\_find\\_primers.pl](http://www.flyrnai.org/cgi-bin/RNAi_find_primers.pl)) and each primer  
324 contained the T7 RNA polymerase promoter sequence  
325 (5'-TAATACGACTCACTATAGGG-3') at the 5'-end (Table 1). The PCR  
326 products were purified using a QIAEXII Gel Extraction Kit (Qiagen). The  
327 purified PCR products were used as templates to produce dsRNA by using the  
328 T7 RiboMAX<sup>TM</sup> Express RNAi System (Promega). The dsRNA products were  
329 purified with RNeasy Mini Kit (Qiagen) and analyzed by 1.2% agarose gel  
330 electrophoresis.

331 Sf9 cells in 12-well plates were transfected with 7.5 µg of dsRNA targeting  
332 NSF, or 7.5 µg of the GFP dsRNA as a negative control. At 24, 48, and 72 h p.t.,  
333 cell viability was determined as described above. NSF knock-down efficiency  
334 was determined by transfecting Sf9 cells with 2 µg of the plasmid  
335 NSF-MycpBlue that expresses Myc-tagged NSF, or co-transfecting Sf9 cells

336 with 2  $\mu$ g of NSF-MycpBlue and either a) 7.5  $\mu$ g of dsRNA targeting NSF or b)  
337 7.5  $\mu$ g dsRNA targeting GFP. At 24 and 48 h p.t., the transfected and  
338 co-transfected cells were collected and the expression of NSF-Myc was  
339 determined by Western blot analysis. Quantities of proteins on Western blots  
340 were estimated by using Quantity One software. For analysis of virus infection,  
341 Sf9 cells were transfected with 7.5  $\mu$ g of dsRNA targeting NSF, or 7.5  $\mu$ g of the  
342 GFP dsRNA. At 48 h p.t., the cells were infected with wild-type (WT) AcMNPV  
343 at an MOI of 5. At 24 h p.i., the supernatants were collected and virus titers  
344 were measured by TCID<sub>50</sub> assays on Sf9 cells.

#### 345 **Analysis of viral gene expression and DNA replication**

346 To determine the effects of dominant-negative NSF proteins on viral gene  
347 expression, Sf9 cells in 6-well plates were co-transfected with 3  $\mu$ g of  
348 pBieGP64 expressing GP64 and 3  $\mu$ g of a plasmid expressing NSF-GFP,  
349 NSF<sup>E329Q</sup>-GFP, NSF<sup>R385A</sup>-GFP, or the control GFP protein. At 12 h p.t., the cells  
350 were infected with the *gp64* knockout virus LacZGUS-*gp64*<sup>ko</sup> at an MOI of 5. At  
351 6 and 24 h p.i., the infected cells were lysed with 0.5% NP-40 in PBS (pH7.4)  
352 and the  $\beta$ -galactosidase or  $\beta$ -glucuronidase activities were measured using the  
353 substrate Chlorophenol red- $\beta$ -D-galactopyranoside (CPRG, Roche Diagnostics  
354 GmbH) or 4-Nitrophenyl  $\beta$ -D-glucuronide (PNPG, Sigma-Aldrich) by  
355 absorbance at 570 nm (CPRG) or 405 nm (PNPG).

356 To evaluate the effects of DN NSF proteins on viral DNA replication, Sf9  
357 cells were co-transfected with the same plasmids described above (3  $\mu$ g of  
358 each), then infected at 12 h p.t. with *gp64* knockout virus LacZGUS-*gp64*<sup>ko</sup>  
359 (MOI=5). At 24 h p.i., total DNA was extracted from infected cells using a  
360 DNeasy blood tissue kit (Qiagen). Viral genomic DNA was quantified by

361 real-time PCR (IQ<sup>TM</sup>5 Multicolor Real-Time PCR Detection System, Bio-Rad).  
362 Each PCR mixture contained 5 µl SYBR<sup>®</sup> Premix ExTaq II (TaKaRa), 1.25 µM  
363 each primer, and 500 pg of the DNA template. The primers, ODV-e56F:  
364 5'-GATCTTCCTGCGGGCCAAACACT-3' and ODV-e56R:  
365 5'-AACAAGACCGCGCCTATCAACAAA-3', were used to amplify a fragment of  
366 183 bp of the AcMNPV ODV-e56 gene as described previously (36). Thermal  
367 cycling conditions were one cycle of 95° for 3min, followed by 40 cycles of 95°  
368 for 10s, and 60° for 45s. A standard curve was generated by a serial dilution of  
369 ODV-e56pGEM, which contains the ODV-e56 ORF (36). AcMNPV genomic  
370 DNA was expressed as numbers of viral DNA copies per cell.

#### 371 **Analysis of virus entry**

372 Sf9 cells in 6-well plates were transfected with 3 µg of the plasmid  
373 GFP-pBlue, NSF-GFPpBlue, NSF<sup>E329Q</sup>-GFPpBlue or NSF<sup>R385A</sup>-GFPpBlue. At  
374 12 h p.t., the cells were pre-chilled at 4° for 30 min and then incubated with  
375 mCherry-labeled virions of AcMNPV-3mC (MOI=10 or 20 TCID<sub>50</sub>) at 4° for 1 h.  
376 After removing the virus inoculum, cells were washed twice with cold TNMFH  
377 medium and shifted to 27° for 60 min. One set of cells (which infected with an  
378 MOI of 10) were used for extraction of total DNA and viral genomic DNA was  
379 quantified by real-time PCR as described above. The other set of cells (which  
380 infected with an MOI of 20) was fixed with 3.7% paraformaldehyde in PBS (pH  
381 7.4) and analyzed by confocal microscopy as described below.

#### 382 **Analysis of virus egress**

383 To examine the effects of DN NSF on infectious budded virion production,  
384 Sf9 cells in 6-well plates were transfected with 3 µg of recombinant AcMNPV  
385 bacmid GFP-Bac, NSF-GFPBac, NSF<sup>E329Q</sup>-GFPBac, or NSF<sup>R385A</sup>-GFPBac,



386 which express NSF or control genes under an *ie1* promoter. At 24 h p.t.,  
387 GFP-positive cells were counted under an epifluorescence microscope (Nikon  
388 Eclipse Ti) to evaluate the transfection efficiency. Transfected cells were also  
389 solubilized with 0.5% NP-40 in PBS (pH 7.4) and GUS activities were  
390 measured as described above. The cell supernatants were collected and  
391 infectious virus titers were determined by TCID<sub>50</sub> assays on Sf9 cells.

### 392 **Confocal microscopy and imaging**

393 Transfected and/or infected Sf9 cells were prepared on glass coverslips  
394 and fixed with 3.7% paraformaldehyde in PBS (pH 7.4) for 10 min and  
395 permeabilized with 0.05 % Triton X-100 in PBS (pH 7.4) for 1 min. The nuclei  
396 were then stained with 1 µg/ml Hoechst 33258 (Invitrogen) for 8 min. After  
397 washing four times with PBS (pH 7.4), the cells were mounted on slides in  
398 Fluoromount-G reagent (Southern Biotech). Images were collected on a Nikon  
399 A1R confocal microscope (Nikon Instruments Inc., Melville, NY, USA) with a  
400 60x oil immersion objective (NA 1.4). GFP was excited with a blue argon ion  
401 laser (488 nm), and emitted light was collected between 480 and 520 nm.  
402 mCherry was excited with an orange helium-neon laser (594 nm), and emitted  
403 light was collected from 580 to 650nm. Hoechst 33258 was excited with UV  
404 light at approximately 350 nm, and emitted light was collected from 400 nm to  
405 450 nm. GFP and mCherry signals were collected separately from the Hoechst  
406 33258 signal and later superimposed. Images were processed using Nikon  
407 NIS-Elements AR software (version 4.0), and Adobe Photoshop CC (version  
408 14.0) (Adobe Systems).

### 409 **cELISA, immunofluorescence, and syncytium formation assay**

410 Sf9 cells in 12-well plates were transfected with 2.5 µg of the bacmid

411 (GFP-Bac, NSF<sup>E329Q</sup>-GFPBac, or NSF<sup>R385A</sup>-GFPBac), or 0.5-2.5 µg  
412 NSF-GFPBac. At 24 h p.t., the supernatant was collected and the infectious  
413 BV titers were determined by TCID<sub>50</sub> assay. Two sets of transfected cells were  
414 separately fixed with either 0.5% glutaraldehyde or 3.7% paraformaldehyde,  
415 and analyzed by cELISA or immunofluorescence using anti-GP64 monoclonal  
416 antibodies AcV5 or AcV1, respectively. Another set of cells was treated with  
417 PBS (pH 5.0) for 3 min to induce syncytium formation. The cells in syncytia  
418 (containing ≥5 nuclei) were scored. ELISA, immunofluorescence, and  
419 syncytium formation assays were carried out as described previously (38).

#### 420 **Transmission electron microscopy**

421 Sf9 cells in 6-well plates were transfected with 6 µg of each bacmid  
422 (NSF-GFPBac, NSF<sup>E329Q</sup>-GFPBac, or NSF<sup>R385A</sup>-GFPBac). At 48 h p.t., the  
423 cells were harvested by centrifugation (500 g, 10 min) and fixed with 2.5%  
424 glutaraldehyde in PBS (pH 7.4) overnight at 4°. Cells were then washed five  
425 times with PBS buffer (0.1 M, pH 7.2) and stained with 1% osmium tetroxide in  
426 PBS buffer (0.2 M, pH 7.2) for 2 h at 4°. After rinsing five times in PBS buffer  
427 (0.1 M, pH 7.2), the samples were dehydrated stepwise with a gradient of  
428 ethanol from 30% to 100%. The samples were then embedded in Epon-812  
429 and dried for about 48 h at 55°. Ultrathin sections were prepared and stained  
430 with lead citrate and uranyl acetate. Images were collected with a HT7700  
431 transmission electron microscope (Hitachi, Ltd. Japan).

#### 432 **Coimmunoprecipitation**

433 Sf9 cells in 12-well plates were transfected or co-transfected with the  
434 plasmids expressing HA-tagged GP41 and/or c-Myc tagged GP41 or Lef3, or  
435 c-Myc tagged NSF and/or HA-tagged viral proteins (2 µg of each plasmid). At

436 36 h p.t., the cells were lysed in RIPA buffer (0.1% SDS, 50mM Tris pH 8.0,  
437 150 mM NaCl, 5mM EDTA, 0.5% Sodium deoxycholate, 1% NP-40) containing  
438 protein inhibitor cocktail (Roche) at 4° for 10 min. Then, the supernatant was  
439 collected and debris removed by centrifugation (15,000 *g*, 15 min, 4°). For  
440 immunoprecipitation, the lysate supernatants were mixed with anti-HA  
441 monoclonal antibodies for 4 h at 4°, then the mixture was incubated with  
442 Protein G agarose beads (Pierce) overnight at 4°. After pelleting and washing  
443 twice with RIPA buffer, the agarose beads were resuspended with 1x  
444 SDS-PAGE gel loading buffer (2% SDS, 10% glycerol, 2%  $\beta$ -mercaptoethanol,  
445 0.02% bromophenol blue, 0.05 M Tris, pH 6.8), heated at 100° for 5 min, and  
446 analyzed in 10% or 15% SDS-PAGE and Western blot.

#### 447 **Bimolecular fluorescence complementation (BiFC) assay**

448 Sf9 cells in 12-well plates were co-transfected with the BiFC plasmid pairs  
449 (2  $\mu$ g of each plasmid) expressing the specific protein fused with the N- or C-  
450 terminus of mCherry (Nm or Cm, respectively). At 36 h p.t., bimolecular  
451 fluorescent complementation was examined by observing mCherry  
452 fluorescence in transfected cells with a Nikon Eclipse Ti epifluorescence  
453 microscope. In five randomly selected representative fields, the numbers and  
454 percentages of mCherry-positive cells were calculated for each pair of  
455 constructs. The protein pair associations were estimated by the ratio of the  
456 number of fluorescent cells in the field compared to the total number of cells in  
457 that field as described previously (41). Expression of the target proteins was  
458 confirmed in transfected cells by Western blot analysis.

#### 459 **BV purification**

460 The purification of budded virions (BV) was performed as described

461 previously (36). Briefly, Sf9 cells in 6-well plates were transfected with 6  $\mu$ g  
462 DNA of NSF-MycBac. At 72 h post transfection (p.t.), the infected cell  
463 supernatants were collected and cell debris removed by centrifugation at 4° for  
464 10 min at 3,000 g. The supernatant was loaded onto a 25% (wt/vol) sucrose  
465 cushion, and centrifuged (4°, 90 min, 28000 rpm, Himac P28S rotor). Virus  
466 pellets were resuspended in PBS (pH 6.2) and overlaid onto a 30-55% (wt/vol)  
467 continuous sucrose gradient, and centrifuged (4°, 90 min, 28000 rpm, Himac  
468 P40ST rotor). The virus fraction was collected and diluted (1:10) with PBS (pH  
469 6.2), and centrifuged at 28000 rpm for 90 min at 4° (Himac P40ST rotor). BV  
470 pellets were resuspended in PBS (pH 6.2) with protease inhibitor cocktail  
471 (Roche) and subjected to Western blot analysis.

#### 472 **Western blot analysis**

473 Virion and cell lysates were separated on 6%, 10% or 15% reducing or  
474 non-reducing polyacrylamide gels and transferred to PVDF membrane  
475 (Millipore) as described previously (42). GFP, GFP-tagged proteins,  
476 c-Myc-tagged proteins, and AcMNPV VP39 were separately detected with  
477 anti-GFP (GenScript), anti-Myc (EarthOx, L.L.C.), or anti-VP39 polyclonal  
478 antibodies (43), HA-tagged proteins,  $\beta$ -glucuronidase (GUS), or actin were  
479 detected with anti-HA (EarthOx, L.L.C.), anti-GUS (BGI), or anti- $\beta$ -actin  
480 monoclonal antibodies (Abbkine). Immunoreactive proteins were visualized  
481 using alkaline phosphatase-conjugated anti-mouse or anti-rabbit IgG antibody  
482 and nitroblue tetrazolium/5-bromo-4-chloro-3-indolylphosphate (NBT/BCIP,  
483 Promega).

#### 484 **Accession number**

485 The *Spodoptera frugiperda* NSF gene was deposited under GenBank

486 accession number KY548397.

## 487 **Results**

### 488 **Expression profiles of SNARE genes upon AcMNPV infection**

489 As a first step, we performed a comprehensive comparison of SNARE  
490 protein components in yeast, humans, and insects. We found that most of the  
491 components of the cellular SNARE machinery are evolutionarily conserved  
492 across these eukaryotic species (Table 3). Insect genes encoding SNARE  
493 components appear to more closely mirror the yeast genome in terms of  
494 SNARE gene numbers. In contrast to the rather large expansion of SNARE  
495 genes observed in the human genome, we identified only one SNARE gene  
496 (the ortholog of yeast Sec17) that was expanded in the six insect Orders (Table  
497 3). In addition, several yeast SNARE genes were not identified in insect  
498 genomes, and these include Sft1, Vam3, Vam7, and Snc1/Snc2. In a recent  
499 transcriptome analysis of AcMNPV-infected *Trichoplusia ni* cells (Tnms42),  
500 expression profiles were generated for host genes throughout the AcMNPV  
501 infection cycle (33). We therefore analyzed the expression profiles of host  
502 SNARE gene orthologs (Fig. 1 and Table S1) in uninfected and  
503 AcMNPV-infected cells. Upon AcMNPV infection, more than 70% of the  
504 SNARE genes (17/23) were up-regulated (>1-fold change in transcript  
505 abundance upon AcMNPV infection). Of these genes, the expression levels of  
506 Bet1, Sec20, Sec22, SNAP-29, Syb, and Use1 were increased >2 fold in  
507 AcMNPV infected cells. Overall, we found that in the early stages of AcMNPV  
508 infection, most of the SNARE genes were either up-regulated or maintained  
509 their expression levels (Fig. 1, Table S1).

510 In eukaryotic cells, NSF forms a regulatory complex with  $\alpha$ -SNAP to unfold

511 and recycle SNARE proteins (9). Although the  $\alpha$ -SNAP transcript is  
512 up-regulated in the very early stage of AcMNPV infection (1-6 h p.i.) in *T.ni*  
513 cells, the transcript level of NSF remained stable, and slightly decreased by 6 h  
514 p.i. (Fig. 1E, Table S1). To determine the transcript levels of NSF in  
515 AcMNPV-infected Sf9 cells, we first identified the Sf9 NSF mRNA (from  
516 Spodobase) and used quantitative real-time PCR to measure NSF transcript  
517 levels from uninfected and infected Sf9 at various times post infection. As  
518 shown in Figure 2, AcMNPV infection significantly up-regulated the transcript  
519 levels of NSF at 1 and 3 h p.i. Similar to observations in AcMNPV-infected  
520 Tnms42 cells, the transcript levels of NSF were substantially decreased at 6 h  
521 p.i. Combined, these transcript data suggest that the cellular SNARE system  
522 may be important in AcMNPV infection or that specific SNARE components  
523 may play important roles.

#### 524 **Analysis of NSF from Sf9 cells**

525 Because the SNARE system may be important for successful AcMNPV  
526 infection, we asked whether NSF, a key regulator of SNARE activity, is  
527 required for AcMNPV replication. To isolate the NSF gene from Sf9 cells, we  
528 designed gene-specific primers targeting the 5' and 3' ends of the NSF ORF  
529 based on partial EST sequences of *S. frugiperda* NSF obtained from Blast  
530 searches. We then amplified and cloned the NSF ORF from Sf9 cells. The Sf9  
531 NSF gene contains a 2241 bp ORF encoding a 746 amino acid protein with a  
532 predicted molecular weight of 82.6 kDa. Sf9 NSF had highest amino acid  
533 sequence identity to NSF of *B. mori* (92.25%) and is highly conserved with  
534 orthologs from other insect species (71.64%-78.51%) and other eukaryotes  
535 (44.77% similar to yeast NSF and 63.19% similar to human NSF). Mammalian

536 NSF proteins contain several functional domains: an amino-terminal domain  
537 (NSF-N), followed by two homologous domains termed D1 and D2. These  
538 functional domains were predicted to be present in NSF of *Spodoptera*  
539 *frugiperda* (Sf9 cells) and other insects (Fig. S1).

#### 540 **Transient expression of WT and DN NSF in Sf9 cells**

541 To generate dominant-negative (DN) forms of Sf9 NSF proteins, two  
542 previously characterized point mutations (E329Q and R385A) that each  
543 abolish ATP hydrolysis activity in human NSF (10, 12) were introduced into Sf9  
544 NSF (Fig. 3A and S1, NSF<sup>E329Q</sup> and NSF<sup>R385A</sup>). To confirm the expression and  
545 subcellular localization of NSF constructs, wild-type (WT) and DN NSFs were  
546 fused with GFP at the C-terminus and inserted into a plasmid under the control  
547 of an AcMNPV *ie1* promoter. These constructs were transiently expressed in  
548 Sf9 cells (Fig. 3B-C). A plasmid expressing GFP under the same promoter  
549 (gfppBlue) was used as a control. Transient expression of each construct was  
550 confirmed by Western blot analysis with an anti-GFP antibody (Fig. 3B) and by  
551 epifluorescence and confocal microscopy (Fig. 3C). GFP-tagged WT NSF was  
552 distributed diffusely throughout the cytoplasm. In contrast, NSF<sup>E329Q</sup>-GFP and  
553 NSF<sup>R385A</sup>-GFP showed a generally cytoplasmic punctate distribution in  
554 transfected Sf9 cells (Fig. 3C) similar to that observed previously with human  
555 NSF DN constructs (44). To determine potential general effects of  
556 NSF<sup>E329Q</sup>-GFP and NSF<sup>R385A</sup>-GFP on the proliferation of Sf9 cells, the viability  
557 of cells expressing each construct was measured. At 12, 24, or 36 h  
558 post-transfection (p.t.), the viability of Sf9 cells transiently expressing DN NSF  
559 proteins was similar to that of cells expressing WT NSF or GFP (Fig. 3D).  
560 These data suggest that transient expression of DN NSF proteins over this

561 short time period did not result in a measurable negative effect on the viability  
562 of Sf9 cells.

### 563 **Effects of DN NSF expression or NSF knock-down on infectious AcMNPV** 564 **production**

565 To determine whether NSF is required for productive AcMNPV infection, we  
566 first used a viral complementation assay to examine AcMNPV replication in the  
567 presence of DN NSF proteins. Because all cells do not become transfected  
568 and express the DN constructs in transient transfection assays, the  
569 complementation assay insures that productive viral replication can occur only  
570 in cells that are productively transfected and express both the DN NSF  
571 construct and WT GP64 (which complements the *gp64* knockout and permits  
572 production of infectious BV). In this assay, Sf9 cells were co-transfected with  
573 two plasmids: one expressing GP64 and another expressing either GFP, NSF,  
574 or DN NSF constructs (NSF<sup>E329Q</sup>-GFP or NSF<sup>R385A</sup>-GFP). At 12 h p.t., the  
575 transfected cells were infected with the *gp64* knockout virus  
576 (mCherryGUS-*gp64*<sup>ko</sup>) at an MOI of 1 or 5. At 24 h p.i., the cell culture  
577 supernatants were harvested and the infectious virus titers were determined  
578 on a GP64-expressing cell line (Sf9<sup>Op1D</sup>) that complements the *gp64* knockout  
579 virus. (Note: Virus produced from the transfected cells should contain GP64  
580 produced from the plasmid, but the virus cannot spread from cell to cell in an  
581 endpoint titration assay. Thus the Sf9<sup>Op1D</sup> cell line is used for the TCID<sub>50</sub> assay,  
582 to detect virions produced in the transfection-infection assay.). As shown in Fig.  
583 4B, the production of infectious AcMNPV is significantly reduced (>97%  
584 reduction at an MOI of 5) in the presence of either DN NSF construct,  
585 NSF<sup>E329Q</sup>-GFP or NSF<sup>R385A</sup>-GFP. In contrast, the expression of WT NSF had



586 no effect on infectious virus production compared with that in cells expressing  
587 GFP. A similar result was observed when cells were infected at an MOI of 1. In  
588 these co-transfected and infected Sf9 cells, both GP64 and each of the NSF  
589 protein constructs were expressed at substantial levels (Fig. 4A). Additionally,  
590 in parallel experiments a similar reduction of infectious AcMNPV production  
591 was also observed in another lepidopteran cell line, *T. ni* High 5 cells, in the  
592 presence of DN NSF proteins (data not shown).

593 To extend our observations, we used a dsRNA-based RNAi approach to  
594 evaluate the effect of an NSF knock-down on the production of infectious  
595 AcMNPV. Sf9 cells were mock transfected or transfected with a dsRNA specific  
596 for Sf9 NSF or a dsRNA targeting a GFP control gene. Knock-down  
597 efficiencies for NSF were approximately 16.2% (24 h p.t.) and 74.6% (48 h p.t.)  
598 (Fig. 4C), and transfection with the dsRNA targeting NSF or GFP resulted in no  
599 significant change in the viability of Sf9 cells at 24, 48, and 72 h p.t. (data not  
600 shown). Similar to the results from DN NSF expression, we found that  
601 depletion of NSF also resulted in a dramatic reduction in the production of  
602 infectious AcMNPV (Fig. 4D). Together, these results suggest that functional  
603 NSF appears to be important for the efficient replication of AcMNPV.

#### 604 **Effects of DN NSF on early stages of AcMNPV infection**

605 Budded virions of AcMNPV enter host cells via clathrin-mediated  
606 endocytosis (26), which is regulated in part, by the coordinated action of  
607 several SNARE proteins (Table 3) (4). The negative effects of the DN NSF and  
608 the NSF knock-down on AcMNPV BV production could result from disruption of  
609 the viral infection cycle at an early stage of infection, possibly by interfering  
610 with the transport of virions within endosome during entry. To examine this

611 possibility, Sf9 cells were co-transfected with two plasmids expressing: a)  
612 GP64 and b) one of the following proteins: NSF-GFP, NSF<sup>E329Q</sup>-GFP,  
613 NSF<sup>R385A</sup>-GFP, or GFP. At 12 h p.t., the cells were infected with a *gp64*  
614 knockout virus (LacZGUS-*gp64*<sup>ko</sup>) that contains two reporter genes: LacZ and  
615 GUS, which are controlled by the AcMNPV *ie1* early/late promoter and *p6.9*  
616 late promoter, respectively. At early and later times in the infection cycle, the  
617 transfected and infected cells were lysed and relative  $\beta$ -Gal and GUS activities  
618 were measured. As shown in Figures 5A and B, the activities of both  $\beta$ -Gal and  
619 GUS were similar in cells expressing control protein GFP or NSF-GFP.  
620 However, in the presence of the two DN NSF proteins (NSF<sup>E329Q</sup>-GFP or  
621 NSF<sup>R385A</sup>-GFP), both  $\beta$ -Gal and GUS activities were significantly reduced  
622 when compared with the controls (Fig. 5A and B). In addition, viral genomic  
623 DNA was isolated from transfected-infected cells (under the same conditions),  
624 and viral genomic DNA replication efficiency was measured by quantitative  
625 real-time PCR detection of genomic DNA. The results showed that the  
626 transient expression of DN NSF proteins (NSF<sup>E329Q</sup>-GFP or NSF<sup>R385A</sup>-GFP)  
627 resulted in a significantly reduced level of viral genomic DNA (Fig. 5C).  
628 Because early and late gene expression and viral DNA replication were all  
629 reduced, these results suggest that the presence of DN NSF proteins inhibit  
630 viral infection at a step prior to early gene expression, possibly inhibiting  
631 trafficking of the entering virion from the cell surface to the nucleus.

### 632 **Effects of DN NSF on internalization and transport of AcMNPV BV during** 633 **entry**

634 Several SNARE proteins and NSF (which regulates their function) play  
635 important roles in endocytosis by mediating vesicle fusion (4, 45). To examine

636 whether viral entry by endocytosis involved SNARE-mediated fusion events,  
637 we examined mCherry-tagged BV entry in the presence of WT or DN NSF  
638 proteins. We first transfected Sf9 cells with a plasmid expressing either WT  
639 NSF, a DN-NSF, or GFP. After a 12 h period of expression, cells were  
640 incubated with mCherry-labeled AcMNPV virions (AcMNPV-3mC) at 4° for 60  
641 min to permit virus adsorption at the cell surface. After removing the viral  
642 inoculum and washing the cells twice with cold medium, the temperature was  
643 raised to 27° and cells incubated for 60 min. Internalized virus was quantified  
644 by qRT-PCR measurements of viral genomic DNA. Internalized viral DNA was  
645 dramatically reduced in cells expressing DN NSF proteins (61.8% and 65.0%  
646 reduction in NSF<sup>E329Q</sup>-GFP and NSF<sup>R385A</sup>-GFP expressing cells, respectively)  
647 as compared with cells expressing the WT NSF protein or the control GFP (Fig.  
648 6A). In addition to qRT-PCR, the transport of virions was also analyzed by  
649 confocal microscopy (Fig. 6B). In control cells expressing WT NSF or GFP, the  
650 mCherry labeled nucleocapsids were observed as small but discrete foci of  
651 fluorescence distributed more evenly throughout the cytoplasm, and some  
652 were observed within the nucleus. In contrast, the mCherry-labeled  
653 nucleocapsids in cells expressing DN NSF proteins (NSF<sup>E329Q</sup>-GFP and  
654 NSF<sup>R385A</sup>-GFP) were observed aggregated in the cytoplasm in discrete foci  
655 which likely represent endosomes. Interestingly, the aggregated  
656 mCherry-tagged nucleocapsids were not colocalized with GFP-tagged DN  
657 NSF proteins (Fig. 6B, lower panels, GFP vs. mCherry). Thus, while qPCR  
658 results suggested that binding and entry were affected by DN NSF expression,  
659 confocal microscopy show that transport of AcMNPV nucleocapsids was also  
660 disrupted. Overall, these data suggest that NSF is required for efficient

661 internalization and intracellular transport of AcMNPV BV during entry.

662 **Is NSF is required for efficient egress of infectious AcMNPV?**

663 In the studies described above, we found that expression of DN NSF  
664 proteins in Sf9 cells led to inefficient internalization and transport of AcMNPV  
665 BV. Therefore, to study the role of NSF in virion egress and to circumvent the  
666 negative effects on virus entry, we initiated infections by transfecting Sf9 cells  
667 with AcMNPV bacmid DNA. Each AcMNPV bacmid DNA expressed a WT or  
668 DN NSF protein (tagged with GFP) plus a reporter GUS protein. NSF  
669 constructs were expressed from the viral genome under the control of the  
670 AcMNPV *ie1* early/late promoter, and the GUS reporter gene was expressed  
671 from the *p6.9* late promoter. Thus DN-NSF proteins were expressed in the  
672 early phase of infection prior to egress, which occurs during the late phase  
673 after assembly of progeny nucleocapsids. Because NSF is a homo-hexamer (9)  
674 that is continually assembling and disassembling, DN NSF expressed early  
675 should inactivate the function of pre-existing wild-type NSF. At 24 h  
676 post-transfection, GFP-positive cells were scored to evaluate transfection  
677 efficiency and expression of the NSF-GFP fusions. In parallel, late  
678 promoter-driven GUS activity was measured to monitor progression of the viral  
679 infection. As shown in Figure 7, the percentage of GFP-positive cells from  
680 transfections with different bacmids (GFPBac, NSF-GFPBac,  
681 NSF<sup>E329Q</sup>-GFPBac, NSF<sup>R385A</sup>-GFPBac) varied from 35.7% to 38.4% (Fig. 7A).  
682 Also, relative GUS activities measured from the transfected cells lysates from  
683 cells transfected with the same bacmid DNAs were also at similar levels (Fig.  
684 7B). These results indicate that, in cells transfected with the different bacmids  
685 (expressing GFP, NSF-GFP, or DN NSF constructs), transfection efficiencies

686 were approximately equivalent, and in all cases virus infection progressed into  
687 the late phase. Virus titers in supernatants from cells expressing NSF-GFP or  
688 the control GFP protein were both approximately  $2.5 \times 10^5$  TCID<sub>50</sub>/ml. In  
689 contrast, no infectious AcMNPV BV was detected in supernatants (24 h p.t.)  
690 from cells expressing DN NSF constructs NSF<sup>E329Q</sup>-GFP or NSF<sup>R385A</sup>-GFP (Fig.  
691 7C). Thus, these data suggest that NSF is required for the egress and  
692 production of infectious AcMNPV BV.

### 693 **Is cell surface expression of functional GP64 dependent on NSF?**

694 Since the viral envelope glycoprotein GP64 is necessary for production of  
695 infectious BV (42) and is trafficked through the secretory pathway, the SNARE  
696 system may be important for GP64 trafficking. Therefore, we asked whether  
697 DN NSF proteins affected expression, transport, and/or cell surface  
698 localization of GP64 in the context of a viral infection. To address this question,  
699 we transfected Sf9 cells with AcMNPV bacmid DNA expressing either WT NSF  
700 or DN NSF proteins (both tagged with GFP) as described above. At 24 h p.t.,  
701 the expression of GP64 in these bacmid-transfected Sf9 cells was examined  
702 by Western blot analysis under reducing and non-reducing conditions for  
703 SDS-PAGE. Under non-reducing conditions, GP64 is found as disulfide-linked  
704 trimers of GP64 monomers. Two forms of GP64 trimers (known as Trimer I and  
705 Trimer II) are typically observed in infected cells (46-48). These typical forms of  
706 GP64 were detected in cells expressing DN NSF proteins (NSF<sup>E329Q</sup>-GFP or  
707 NSF<sup>R385A</sup>-GFP), and in cells expressing control proteins: WT NSF-GFP and  
708 GFP (Fig. 8A). The intensities of the trimeric and monomeric GP64 bands were  
709 similar for all bacmid-transfected cells, suggesting that the DN NSF proteins  
710 did not substantially alter the expression, stability, or oligomerization of GP64.

711 Cell surface localized GP64 was examined by cELISA with the AcV5 antibody  
712 and by immunofluorescence analysis with the MAb AcV1, which recognizes  
713 the native neutral-pH conformation of GP64 (49) (Fig. 8B and C). In cells  
714 expressing DN NSF proteins, the cell surface levels of GP64 were reduced to  
715 approximately 40% of that from cells expressing WT NSF or GFP (Fig. 8B).  
716 Although GP64 cell surface levels were significantly reduced in the presence  
717 of DN NSF, the recognition of surface localized GP64 by MAb AcV1 indicates  
718 that GP64 is in the native conformation. To determine whether the presence of  
719 DN NSF proteins affected the fusion activity of GP64 expressed in those cells,  
720 we measured fusion activity of GP64 on cells transfected with bacmids  
721 expressing WT or DN NSF proteins. Because cell surface levels of GP64  
722 varied between the cells expressing WT and DN NSF proteins, and surface  
723 GP64 levels may affect the detection of membrane fusion activity, we initially  
724 generated a standard curve of cell surface levels of GP64 by transfecting Sf9  
725 cells with decreasing quantities of the bacmid that expresses wild-type NSF,  
726 and performing cELISA analysis (Fig. 8B). A parallel standard curve of  
727 pH-triggered membrane fusion levels was generated by transfecting cells with  
728 decreasing quantities of the same bacmid (Fig. 8D, NSF-GFP) and measuring  
729 fusion activity as percentages of cells in syncytial masses. Comparisons of  
730 GP64-mediated fusion activity in cells expressing DN NSF constructs  
731 (NSF<sup>E329Q</sup>-GFP and NSF<sup>R385A</sup>-GFP) with fusion from WT NSF expressing cells  
732 in which GP64 was present at the same levels, show that there was no  
733 apparent effect on GP64-mediated fusion efficiency in the presence of DN NSF  
734 proteins (Fig. 8B, D). Thus, while expression of the DN NSF proteins caused a  
735 moderate decrease in surface levels of GP64, there was no effect on the

736 function of the surface-localized protein.

737 We also examined infectious BV produced from cells transfected with  
738 bacmids expressing WT or DN NSF proteins. When cells were transfected with  
739 the bacmid expressing WT NSF (NSF-GFPBac, 2.5  $\mu$ g) or expressing a control  
740 GFP protein, we detected infectious BV titres of approximately  $1.5 \times 10^5$   
741 TCID<sub>50</sub>/ml. However, in supernatants from cells transfected with DN NSF  
742 constructs NSF<sup>E329Q</sup>-GFPBac and NSF<sup>R385A</sup>-GFPBac, no infectious BV was  
743 detected (Fig. 8E). Thus while NSF may play a minor role in intracellular  
744 transport and cell surface localization of GP64, the defect in infectious  
745 AcMNPV BV production in the presence of DN NSF proteins was dramatic,  
746 and was not explained by the modestly lower cell surface levels of GP64.

#### 747 **Effects of DN NSF on nucleocapsid egress from the nuclear membrane**

748 To examine the stage of virion egress that was affected by DN NSF  
749 proteins, we first used transmission electron microscopy (TEM) of  
750 bacmid-transfected cells, to compare the transport of nucleocapsids in control  
751 cells with that in cells expressing DN NSF proteins. In cells expressing WT  
752 NSF-GFP, a typical AcMNPV infection is observed. We observed the typical  
753 presence of an electron-dense virogenic stroma (VS) in the nucleus,  
754 rod-shaped nucleocapsids at the edges of the VS, intranuclear microvesicles  
755 (IM) and nucleocapsids budding from the nuclear membrane (NM) and from  
756 the plasma membrane (PM) (Fig. 9A-D). Cells expressing DN NSF proteins  
757 (NSF<sup>E329Q</sup>-GFP and NSF<sup>R385A</sup>-GFP) also showed the VS, abundant  
758 rod-shaped nucleocapsids, numerous IM, and nucleocapsids associated with  
759 IM in the nuclei (Fig. 9E, F, I, J). However, no progeny nucleocapsids were  
760 observed budding from the plasma membrane (Fig. 9G and K). Interestingly, in

761 cells expressing DN NSF proteins, some progeny nucleocapsids were  
762 observed budding through the inner nuclear membrane (INM) but the INM  
763 enclosed nucleocapsids appeared to be trapped within a perinuclear space  
764 formed by the inner nuclear membrane and the deformed outer nuclear  
765 membrane (Fig. 9G, H, K, L). Combined with the absence of BV production in  
766 the presence of DN NSF, these results suggest that functional NSF could be  
767 important directly or indirectly, for transit of progeny nucleocapsids across the  
768 nuclear membrane.

#### 769 **Association of NSF with viral proteins**

770 Viruses in the family *Baculoviridae* contain a set of about 37 “core” genes  
771 that are conserved in most or all sequenced baculovirus genomes (22). Recent  
772 studies reported that some of these baculovirus core proteins and some of the  
773 highly conserved viral proteins are important for the release of progeny  
774 nucleocapsids from nuclei (50-57). These proteins include Ac11, Ac76, Ac78,  
775 Ac80 (GP41), Ac93, Ac103, Ac142, and Ac146. A similar defect in infectious  
776 AcMNPV production, combined with the aberrant nuclear structures observed  
777 at the nuclear membrane (both caused by DN NSF proteins) suggests the  
778 possibility that NSF may also be involved in egress of nucleocapsids from the  
779 nucleus, perhaps associating with some of the above baculovirus highly  
780 conserved or core proteins. To test this hypothesis, an immunoprecipitation  
781 assay was used to examine the potential association between NSF and each  
782 of the above viral proteins. We selected AcMNPV GP41 and Lef3 as control  
783 proteins, as it was previously demonstrated that GP41 interacts with itself but  
784 does not interact with Lef3 (58). Sf9 cells were co-transfected with two  
785 plasmids: one expressing an HA-tagged viral protein, and another expressing



786 NSF-Myc. At 36 h p.t., the cells were lysed and proteins were  
787 immunoprecipitated with an anti-HA MAb. Expression of the HA-tagged and  
788 Myc-tagged proteins was confirmed by Western blot using appropriate  
789 antibodies (Fig. 10). Of the 8 viral proteins examined, we found that 5  
790 co-immunoprecipitated NSF, suggesting that viral proteins Ac76, Ac78, GP41,  
791 Ac93, and Ac103 may either interact with NSF or may be found in a complex  
792 that includes NSF (Fig. 10).

793 To extend the results from co-immunoprecipitation studies, we further  
794 examined the possible associations of NSF and viral proteins using a  
795 bimolecular fluorescence complementation assay (BiFC) in living cells. Sf9  
796 cells were co-transfected with two plasmids, separately expressing NSF and  
797 one of the viral proteins, with each as a fusion with the N- or C-terminal domain  
798 of mCherry (referred to as Nm or Cm, respectively). Initially, to verify the  
799 specificity of the mCherry-based BiFC system, we also selected AcMNPV  
800 GP41 and Lef3 as candidate bait and prey proteins. By co-expressing  
801 GP41-HA-Nm with either GP41-Myc-Cm or Lef3-Myc-Cm (Nm and Cm  
802 represent N- and C-terminal fragments of mCherry, respectively), we observed  
803 mCherry fluorescence complementation in approximately 50% of the cells  
804 co-transfected with GP41-HA-Nm and GP41-Myc-Cm plasmids (Fig. 11A,  
805 lower right panels). In contrast, fluorescence was not detected in cells  
806 co-expressing GP41-HA-Nm and Lef3-Myc-Cm, even though both of the  
807 fusion proteins were expressed (Fig. 11A, lower right panels). In cells  
808 co-expressing NSF-HA-Nm in combination with Cm-tagged viral proteins, BiFC  
809 fluorescence was observed between combinations of NSF and Ac76, Ac78,  
810 GP41, Ac93, or Ac103, the same 5 proteins identified in Co-IP studies. The

811 percentage of fluorescent cells was highest (40-50%) in cells co-expressing  
812 NSF-HA-Nm with GP41-Myc-Cm or Ac93-Myc-Cm (Fig. 11B). Lower  
813 percentages of fluorescent cells (5-18%) were observed when NSF-HA-Nm  
814 was co-expressed with Ac76-Myc-Cm, Ac78-Myc-Cm, or Ac103-Myc-Cm.  
815 While Western blot analysis showed that all of the fusion proteins were  
816 expressed in co-transfected Sf9 cells, we observed no BiFC fluorescence in  
817 cells co-expressing NSF-HA-Nm with constructs Ac11-Myc-Cm,  
818 Ac142-Myc-Cm, and Cm-Myc-Ac146. (Note: Two different size bands were  
819 detected in Western blots for Ac76-Myc-Cm and Cm-Myc-Ac146 and this  
820 phenomenon has been described previously (53, 54)). Similar BiFC  
821 fluorescence results were observed by reciprocal protein fusions of Nm fused  
822 to viral proteins and Cm fused with NSF (data not shown). Thus, our initial  
823 Co-IP results were confirmed in BiFC experiments in which associations occur  
824 and are detected within live cells. While these data may suggest  
825 protein-protein interactions, BiFC interactions can occur at distances of up to 7  
826 nm and therefore are not definitive evidence of direct protein-protein  
827 interactions. Thus, combined with effects of DN NSF on virus egress, these  
828 Co-IP and BiFC studies suggest that the baculovirus conserved (core)  
829 structural proteins (Ac76, Ac78, GP41, Ac93, and Ac103) are closely  
830 associated with NSF, and complexes of these proteins with cellular NSF may  
831 be involved in AcMNPV egress.

### 832 **Association of NSF with AcMNPV BV**

833 Because NSF is important for efficient entry and egress of AcMNPV BV,  
834 and is closely associated with conserved viral structural proteins, this  
835 suggested that NSF might be assembled into BV during the maturation

836 process. To examine this possibility, Sf9 cells were transfected with AcMNPV  
837 bacmid DNA expressing c-Myc-tagged NSF and a GUS reporter (NSF-MycBac)  
838 and BV preparations were probed for the presence of NSF-Myc by Western  
839 blot analysis. While a negative control ( $\beta$ -glucuronidase, GUS) was not  
840 detected in BV, Myc-tagged NSF was detected in both purified BV and cell  
841 lysates (Fig. 12, NSF). Positive controls GP64 and VP39 were also detected in  
842 both cell lysates and BV. A role for NSF in BV is not known but it is possible  
843 that NSF in the virion could play a role during entry, or that NSF may be  
844 assembled into the BV fortuitously during virion egress.

#### 845 **Discussion**

846 The infection of insect cells by baculoviruses involves a complex interplay  
847 between cell and virus (32, 33, 59-61). Analysis of transcriptome data from  
848 AcMNPV-infected *Trichoplusia ni* Tmns42 cells (33), showed that early in the  
849 infection, many host genes are up-regulated immediately following virus  
850 inoculation, and among these are a number of SNARE-encoding genes (Fig. 1,  
851 Table 3). SNARE proteins function as protein complexes that mediate fusion  
852 between intracellular transport vesicles and membrane-bound compartments  
853 and they are important in endocytosis, ER and Golgi trafficking, and the  
854 secretory pathway (1). The activity of the SNARE system is regulated by a  
855 complex that is formed by NSF and  $\alpha$ -SNAP (9). In AcMNPV infected Tmns42  
856 cells,  $\alpha$ -SNAP and a number of SNARE-related genes are slightly to  
857 moderately up-regulated early after infection and then decline as infection  
858 progresses (Fig. 1). The levels of NSF transcripts are not increased but  
859 decrease gradually after infection. For comparison, we examined the transcript  
860 levels of NSF in AcMNPV-infected Sf9 cells and found that at 1 and 3 h p.i.

861 NSF transcripts were moderately elevated, but had decreased by 6 h p.i. (Fig.  
862 2). It is unclear whether these cell line differences are significant. However,  
863 because of their critical roles in cells, we asked whether they may also be  
864 important for productive viral infection. During entry, AcMNPV nucleocapsids  
865 are typically trafficked to the nucleus within approximately 1 h after inoculation  
866 (29, 62). During this time, the cellular SNARE system components should be  
867 fully intact and functional. We found that general disruption of the SNARE  
868 machinery in insect cells (by overexpressing DN NSF or by down-regulating  
869 NSF using RNAi) resulted in dramatically reduced infectious AcMNPV  
870 production. To understand how viral replication was constrained, we examined  
871 the roles of NSF in both entry and egress.

872 Budded virions of AcMNPV enter host cells via clathrin-mediated  
873 endocytosis (26, 63). Endosomes are then trafficked within the cell, and during  
874 this process they are gradually acidified. The decreasing pH within endosomes  
875 triggers a conformational change in the major viral envelope glycoprotein  
876 (GP64) which mediates membrane fusion and release of the nucleocapsid into  
877 the cytosol (28). Prior studies (64) measuring AcMNPV virion internalization  
878 from the cell surface and transit time within the endosome estimated that virus  
879 entry required approximately 12.5 min from binding until entry into the  
880 endosome, and another approximately 12.5 min before virions become  
881 insensitive to an inhibitor of endosome acidification, indicating release from the  
882 endosome. After endosome release, nucleocapsids are transported to the  
883 nucleus by a mechanism that involves actin polymerization (29). Using DN  
884 NSF constructs, we found that virus entry required a functional SNARE system.  
885 We initially observed that expression of DN NSF resulted in reduced reporter

886 gene expression, reduced viral DNA replication, and lower production of  
887 infectious progeny virus (Fig. 4, 5). Because those results were consistent with  
888 an entry or early phase defect, we examined virion entry more directly, by  
889 tracking the entry of virions containing mCherry-tagged nucleocapsids. In the  
890 presence of DN NSF, we found that mCherry-labeled nucleocapsids were  
891 aggregated in the cytoplasm, indicating that they were not efficiently  
892 transported to the nucleus and were perhaps trapped within endosomes (Fig.  
893 6B).

894 In mammalian cells, the homotypic fusion of early endosomes is driven by a  
895 SNARE complex consisting of an R-SNARE (VAMP4) and Q-SNAREs (Syx6,  
896 Syx13, and Vti1a). Late endosome or endosome–lysosome fusion is mediated  
897 by SNARE complexes consisting of three Q-SNAREs (Syx7, Syx8 and Vti1b)  
898 and one R-SNARE (VAMP7 or VAMP8) (1). (Note: we did not find orthologs of  
899 Syx13 or VAMP8 in sequenced insect genomes, and orthologs of Syx8,  
900 VAMP4, and Vti1b were not found in Lepidoptera insect genomes (Table 3)).  
901 AcMNPV virion entry by receptor mediated endocytosis may require the  
902 function of these or other SNARE complexes. Analysis of gene expression of  
903 SNARE components in AcMNPV-infected *T. ni* cells shows that the  
904 components of these SANRE complexes are either initially up-regulated during  
905 infection or are maintained at constant levels for the first few hours of infection  
906 (Fig. 1). Because AcMNPV BV entry appears to be relatively rapid, preexisting  
907 levels of SNARE complex proteins are likely to be sufficient for BV entry and  
908 changes associated with infection may represent either cellular defensive  
909 reactions to infection, or virus-induced changes associated with requirements  
910 for SNARE complexes at later stages in the infection cycle. The importance of

911 SNARE proteins in entry for some other viruses was demonstrated for certain  
912 negative-stranded RNA viruses, including influenza virus and VSV (20). For  
913 influenza virus and VSV, VAMP8 (which forms the SANRE complex with  
914 endosomal Q-SNAREs Syx7, Syx8 and Vti1b) is recruited to the  
915 virus-containing endosome and promotes virus entry (20). Presently, the series  
916 of events associated with trafficking of baculovirus BV through endosomes  
917 during entry has received little attention, and further studies of the  
918 requirements and/or interactions of cellular factors such as the SNARE  
919 complex proteins should provide new and valuable mechanistic detail on  
920 baculovirus entry.

921 Substantial budding of infectious AcMNPV BV can be detected from  
922 infected cells by 24 h p.i. (22). Early TEM studies showed that progeny  
923 nucleocapsids that assembled in the nucleus, appeared to exit the nucleus by  
924 budding through the nuclear membrane (31). Enveloped nucleocapsids (often  
925 with double membranes presumably derived from inner and outer nuclear  
926 membranes) were observed in the cytoplasm. The observation of free  
927 nucleocapsids in the cytoplasm suggested that these nucleocapsids were  
928 de-enveloped by an unknown mechanism prior to transport to the plasma  
929 membrane, where free nucleocapsids bud through the plasma membrane (31,  
930 65). Recent studies (66) indicate that nucleocapsid trafficking during egress  
931 requires functional kinesin suggesting that either enveloped or free  
932 nucleocapsids move along microtubules during egress. Actin may also be  
933 involved in nucleocapsid egress as actin has been shown to be involved in  
934 nucleocapsid trafficking during entry (29). Expression of DN NSF caused a  
935 modest but significant reduction in surface levels of GP64 (Fig. 8B) and a

936 dramatic reduction in infectious BV production (Fig. 8E). However, GP64  
937 produced in the presence of DN NSF was oligomerized and transported to the  
938 cell surface, and appeared fully functional as a fusion protein (Fig. 8),  
939 suggesting that the modest effects of DN NSF proteins on GP64 trafficking  
940 does not explain the defect in infectious AcMNPV production. We therefore  
941 used TEM to further examine the effects of DN NSF proteins on egress. When  
942 examining the nuclear membranes in the late phase of infection, we found that  
943 the presence of DN NSF proteins resulted in large perinuclear spaces formed  
944 by the INM and a deformed outer nuclear membrane (Fig. 9 G, H, K, and L).  
945 Interestingly, it is known that the SNARE system participates in nuclear  
946 membrane remodeling in *Xenopus laevis* eggs (67). The observation that  
947 AcMNPV nucleocapsids are found in large aberrant perinuclear structures of  
948 the nuclear membranes, suggests that NSF and the SNARE system may be  
949 directly involved in virus-induced remodeling of nuclear membranes during  
950 nucleocapsid egress from the nucleus. Further studies to immunolocalize NSF  
951 and SNARE complexes within infected cells should shed light on whether the  
952 observed phenomena at the nuclear membrane results from direct or indirect  
953 effects. As the mechanism of nuclear egress is not know, it is possible that  
954 SNARE complexes may play a direct role in the pinching off of vesicles  
955 containing progeny nucleocapsids during nuclear egress, or in the release of  
956 nucleocapsids into the cytoplasm after nuclear egress.

957 Because a number of recent studies found that certain highly conserved or  
958 core AcMNPV genes (*ac11*, *ac76*, *ac78*, *ac80* or *gp41*, *ac93*, *ac103*, *ac142*,  
959 and *ac146*), are required for infectious BV production, and knockouts of these  
960 genes result in reduced nucleocapsid egress from the nucleus (50-54, 56, 57,

961 68), we examined their potential associations with NSF. We found that five of  
962 these conserved (core) proteins (Ac76, Ac78, GP41, Ac93, and Ac103)  
963 associated directly or indirectly (perhaps in larger complexes) with NSF.  
964 Predicted structure analysis indicated that, different from the predominant  
965  $\beta$ -sheet composition of Ac11, Ac142, and Ac146, the other five examined viral  
966 proteins only contains 3-6  $\alpha$ -helixes (data not shown). The potential structure  
967 difference might imply the interaction specificity of these viral proteins with NSF.  
968 As such, we might speculate that these viral proteins may associate in a  
969 possible “egress complex” on nuclear membranes. The associations of these  
970 viral proteins with NSF may contribute to the detection of NSF at what appear  
971 to be low levels, in BV preparations (Fig. 12). While NSF was not detected in  
972 BV of AcMNPV in a prior proteomics analysis (32), NSF was identified in BV of  
973 another baculovirus, *Helicoverpa armigera* (Ha)NPV (59). Because of the low  
974 levels of NSF detected in BV, further studies will be required to determine  
975 whether NSF may play a possible functional role in BV.

976 Our studies reveal the importance of the cellular SNARE system in  
977 AcMNPV infection and the critical role of NSF in efficient BV entry, and in  
978 nuclear egress. A hypothetical model (Fig. 13) illustrates the potential  
979 bottlenecks to viral entry and egress and points of potential inhibition by DN  
980 NSF. Further studies will be necessary to define the precise roles of specific  
981 SNARE proteins in AcMNPV infection and to better characterize the  
982 interactions between components of the SNARE system and viral proteins.  
983 Overall, these studies should shed light on understanding the complex  
984 interplay between baculoviruses and the host cells trafficking pathways and  
985 proteins during viral entry and egress.



986 **Acknowledgements**

987 This work was supported by grants from National Key R&D Program of  
988 China (2017YFC1200605), National Natural Science Foundation of China  
989 (31672082, 31272088), and the NCET Program from Ministry of Education of  
990 China (NCET-11-0442) to ZL, and grants from the United States Department of  
991 Agriculture (2015-67013-23281) and National Science Foundation (1354421)  
992 to GB.

993 **References**

- 994 1. **Jahn R, Scheller RH.** 2006. SNAREs--engines for membrane fusion. *Nat Rev Mol Cell Biol*  
995 7:631-643.
- 996 2. **Weber T, Zemelman BV, McNew JA, Westermann B, Gmachl M, Parlati F, Sollner TH,**  
997 **Rothman JE.** 1998. SNAREpins: minimal machinery for membrane fusion. *Cell* **92**:759-772.
- 998 3. **Fasshauer D, Sutton RB, Brunger AT, Jahn R.** 1998. Conserved structural features of the  
999 synaptic fusion complex: SNARE proteins reclassified as Q- and R-SNAREs. *Proc Natl Acad Sci U S A* **95**:15781-15786.
- 1000  
1001 4. **Kloepper TH, Kienle CN, Fasshauer D.** 2007. An elaborate classification of SNARE  
1002 proteins sheds light on the conservation of the eukaryotic endomembrane system. *Mol Biol*  
1003 *Cell* **18**:3463-3471.
- 1004 5. **Sollner T, Bennett MK, Whiteheart SW, Scheller RH, Rothman JE.** 1993. A protein  
1005 assembly-disassembly pathway in-vitro that may correspond to sequential steps of synaptic  
1006 vesicle docking, activation, and fusion. *Cell* **75**:409-418.
- 1007 6. **Mayer A, Wickner W, Haas A.** 1996. Sec18p (NSF)-driven release of sec17p (alpha-SNAP)  
1008 can precede docking and fusion of yeast vacuoles. *Cell* **85**:83-94.
- 1009 7. **Zhao CX, Smith EC, Whiteheart SW.** 2012. Requirements for the catalytic cycle of the  
1010 N-ethylmaleimide-sensitive factor (NSF). *Biochim Biophys Acta* **1823**:159-171.
- 1011 8. **Block MR, Glick BS, Wilcox CA, Wieland FT, Rothman JE.** 1988. Purification of an  
1012 N-ethylmaleimide-sensitive protein catalyzing vesicular transport. *Proc Natl Acad Sci U S A*  
1013 **85**:7852-7856.
- 1014 9. **Zhao M, Brunger AT.** 2016. Recent advances in deciphering the structure and molecular  
1015 mechanism of the AAA+ ATPase N-ethylmaleimide-sensitive factor (NSF). *J Mol Biol*  
1016 **428**:1912-1926.
- 1017 10. **Whiteheart SW, Rossnagel K, Buhrow SA, Brunner M, Jaenicke R, Rothman JE.** 1994.  
1018 N-ethylmaleimide-sensitive fusion protein - a trimeric ATPase whose hydrolysis of ATP is  
1019 required for membrane-fusion. *J Cell Biol* **126**:945-954.
- 1020 11. **Tagaya M, Wilson DW, Brunner M, Arango N, Rothman JE.** 1993. Domain-structure of an  
1021 N-ethylmaleimide-sensitive fusion protein involved in vesicular transport. *J Biol Chem*  
1022 **268**:2662-2666.
- 1023 12. **Matveeva EA, May AP, He P, Whiteheart SW.** 2002. Uncoupling the ATPase activity of the  
1024 N-ethylmaleimide sensitive factor (NSF) from 20S complex disassembly. *Biochemistry*  
1025 **41**:530-536.
- 1026 13. **Nagiec EE, Bernstein A, Whiteheart SW.** 1995. Each domain of the  
1027 N-ethylmaleimide-sensitive fusion protein contributes to its transport activity. *J Biol Chem*  
1028 **270**:29182-29188.
- 1029 14. **Liu ST, Sharon-Friling R, Ivanova P, Milne SB, Myers DS, Rabinowitz JD, Brown HA,**  
1030 **Shenk T.** 2011. Synaptic vesicle-like lipidome of human cytomegalovirus virions reveals a  
1031 role for SNARE machinery in virion egress. *Proc Natl Acad Sci U S A* **108**:12869-12874.
- 1032 15. **Kawabata A, Serada S, Naka T, Mori Y.** 2014. Human herpesvirus 6 gM/gN complex  
1033 interacts with v-SNARE in infected cells. *J Gen Virol* **95**:2769-2777.
- 1034 16. **Ding BB, Zhang GY, Yang XD, Zhang SW, Chen LY, Yan Q, Xu MY, Banerjee AK, Chen**

- 1035 MZ. 2014. Phosphoprotein of human parainfluenza virus type 3 blocks  
1036 autophagosome-lysosome fusion to increase virus production. *Cell Host Microbe* **15**:564-577.
- 1037 17. **Ren H, Elgner F, Jiang B, Himmelsbach K, Medvedev R, Ploen D, Hildt E.** 2016. The  
1038 autophagosomal snare protein syntaxin 17 is an essential factor for the hepatitis c virus life  
1039 cycle. *J Virol* **90**:5989-6000.
- 1040 18. **Joshi A, Garg H, Ablan SD, Freed EO.** 2011. Evidence of a role for soluble  
1041 N-ethylmaleimide-sensitive factor attachment protein receptor (SNARE) machinery in HIV-1  
1042 assembly and release. *J Biol Chem* **286**:29861-29871.
- 1043 19. **Garg H, Joshi A.** 2012. SNAREs in HIV-1 assembly. *Commun Integr Biol* **5**:172-174.
- 1044 20. **Pirooz SD, He SS, Zhang T, Zhang XW, Zhao Z, Oh S, O'Connell D, Khalilzadeh P,**  
1045 **Amini-Bavil-Olyae S, Farzan M, Liang CY.** 2014. UVRAG is required for virus entry  
1046 through combinatorial interaction with the class C-Vps complex and SNAREs. *Proc Natl Acad*  
1047 *Sci U S A* **111**:2716-2721.
- 1048 21. **Meier R, Franceschini A, Horvath P, Tetard M, Mancini R, von Mering C, Helenius A,**  
1049 **Lozach PY.** 2014. Genome-wide small interfering rna screens reveal VAMP3 as a novel host  
1050 factor required for uukuniemi virus late penetration. *J Virol* **88**:8565-8578.
- 1051 22. **Rohrmann GF.** 2013. *Baculovirus Molecular Biology: Third Edition* (Internet). National  
1052 Center for Biotechnology Information (US), Bethesda (MD).
- 1053 23. **Haase S, Sciocco-Cap A, Romanowski V.** 2015. Baculovirus insecticides in Latin America:  
1054 historical overview, current status and future perspectives. *Viruses* **7**:2230-2267.
- 1055 24. **Sun X.** 2015. History and current status of development and use of viral insecticides in China.  
1056 *Viruses* **7**:306-319.
- 1057 25. **van Oers MM, Pijlman GP, Vlak JM.** 2015. Thirty years of baculovirus-insect cell protein  
1058 expression: from dark horse to mainstream technology. *J Gen Virol* **96**:6-23.
- 1059 26. **Long G, Pan XY, Kormelink R, Vlak JM.** 2006. Functional entry of baculovirus into insect  
1060 and mammalian cells is dependent on clathrin-mediated endocytosis. *J Virol* **80**:8830-8833.
- 1061 27. **Li Z, Blissard GW.** 2011. *Autographa californica* multiple nucleopolyhedrovirus GP64  
1062 protein: Roles of histidine residues in triggering membrane fusion and fusion pore expansion.  
1063 *J Virol* **85**:12492-12504.
- 1064 28. **Blissard GW, Wenz JR.** 1992. Baculovirus GP64 envelope glycoprotein is sufficient to  
1065 mediate pH-dependent membrane-fusion. *J Virol* **66**:6829-6835.
- 1066 29. **Ohkawa T, Volkman LE, Welch MD.** 2010. Actin-based motility drives baculovirus transit  
1067 to the nucleus and cell surface. *J Cell Biol* **190**:187-195.
- 1068 30. **Au S, Pante N.** 2012. Nuclear transport of baculovirus: revealing the nuclear pore complex  
1069 passage. *J Struct Biol* **177**:90-98.
- 1070 31. **Fraser MJ.** 1986. Ultrastructural observations of virion maturation in *Autographa-californica*  
1071 nuclear polyhedrosis-virus infected *Spodoptera-frugiperda* cell-cultures. *J Ultrastruct Mol*  
1072 *Struct Res* **95**:189-195.
- 1073 32. **Wang RR, Deng F, Hou DH, Zhao Y, Guo L, Wang HL, Hu ZH.** 2010. Proteomics of the  
1074 *Autographa californica* nucleopolyhedrovirus budded virions. *J Virol* **84**:7233-7242.
- 1075 33. **Chen YR, Zhong SL, Fei ZJ, Gao S, Zhang SY, Li ZF, Wang P, Blissard GW.** 2014.  
1076 Transcriptome responses of the host *Trichoplusia ni* to infection by the baculovirus

- 1077 Autographa californica multiple nucleopolyhedrovirus. *J Virol* **88**:13781-13797.
- 1078 34. **Plonsky I, Cho MS, Oomens AGP, Blissard G, Zimmerberg J.** 1999. An analysis of the  
1079 role of the target membrane on the GP64-induced fusion pore. *Virology* **253**:65-76.
- 1080 35. **Negre V, Hotelier T, Volkoff AN, Gimenez S, Cousserans F, Mita K, Sabau X, Rocher J,**  
1081 **Lopez-Ferber M, d'Alencon E, Audant P, Sabourault C, Bidegainberry V, Hilliou F,**  
1082 **Fournier P.** 2006. SPODOBASE: an EST database for the lepidopteran crop pest Spodoptera.  
1083 *BMC Bioinformatics* **7**:322.
- 1084 36. **Li Z, Blissard GW.** 2012. Cellular VPS4 is required for efficient entry and egress of budded  
1085 virions of Autographa californica multiple nucleopolyhedrovirus. *J Virol* **86**:459-472.
- 1086 37. **Fan JY, Cui ZQ, Wei HP, Zhang ZP, Zhou YF, Wang YP, Zhang XE.** 2008. Split mCherry  
1087 as a new red bimolecular fluorescence complementation system for visualizing protein-protein  
1088 interactions in living cells. *Biochem Biophys Res Commun* **367**:47-53.
- 1089 38. **Li Z, Blissard GW.** 2008. Functional analysis of the transmembrane (TM) domain of the  
1090 Autographa californica multicapsid nucleopolyhedrovirus GP64 protein: substitution of  
1091 heterologous TM domains. *J Virol* **82**:3329-3341.
- 1092 39. **Luckow VA, Lee SC, Barry GF, Olins PO.** 1993. Efficient generation of infectious  
1093 recombinant baculoviruses by site-specific transposon-mediated insertion of foreign genes  
1094 into a baculovirus genome propagated in Escherichia-Coli. *J Virol* **67**:4566-4579.
- 1095 40. **Deng Z, Huang Z, Yuan M, Yang K, Pang Y.** 2014. Baculovirus induces host cell  
1096 aggregation via a Rho/Rok-dependent mechanism. *J Gen Virol* **95**:2310-2320.
- 1097 41. **Webster BM, Colombi P, Jager J, Lusk CP.** 2014. Surveillance of nuclear pore complex  
1098 assembly by ESCRT-III/Vps4. *Cell* **159**:388-401.
- 1099 42. **Oomens AGP, Blissard GW.** 1999. Requirement for GP64 to drive efficient budding of  
1100 Autographa californica multicapsid nucleopolyhedrovirus. *Virology* **254**:297-314.
- 1101 43. **Li L, Li Z, Chen W, Pang Y.** 2007. Cloning, expression of Autographa californica  
1102 nucleopolyhedro virus vp39 gene in Escherichia coli and preparation of its antibody.  
1103 *Biotechnology* **17**:5-7.
- 1104 44. **Zhao C, Matveeva EA, Ren Q, Whiteheart SW.** 2010. Dissecting the  
1105 N-ethylmaleimide-sensitive factor: required elements of the N and D1 domains. *J Biol Chem*  
1106 **285**:761-772.
- 1107 45. **Antonin W, Holroyd C, Fasshauer D, Pabst S, von Mollard GF, Jahn R.** 2000. A SNARE  
1108 complex mediating fusion of late endosomes defines conserved properties of SNARE  
1109 structure and function. *EMBO J* **19**:6453-6464.
- 1110 46. **Kadlec J, Loureiro S, Abrescia NG, Stuart DI, Jones IM.** 2008. The postfusion structure of  
1111 baculovirus gp64 supports a unified view of viral fusion machines. *Nature Struct Mol Biol*  
1112 **15**:1024-1030.
- 1113 47. **Li Z, Blissard GW.** 2010. Baculovirus GP64 disulfide bonds: the intermolecular disulfide  
1114 bond of Autographa californica multicapsid nucleopolyhedrovirus GP64 is not essential for  
1115 membrane fusion and virion budding. *J Virol* **84**:8584-8595.
- 1116 48. **Oomens AG, Monsma SA, Blissard GW.** 1995. The baculovirus GP64 envelope fusion  
1117 protein: synthesis, oligomerization, and processing. *Virology* **209**:592-603.
- 1118 49. **Zhou J, Blissard GW.** 2008. Identification of a GP64 subdomain involved in receptor binding

- 1119 by budded virions of the baculovirus *Autographa californica* multicapsid  
1120 nucleopolyhedrovirus. *J Virol* **82**:4449-4460.
- 1121 50. **Tao XY, Choi JY, Kim WJ, Lee JH, Liu Q, Kim SE, An SB, Lee SH, Woo SD, Jin BR, Je**  
1122 **YH.** 2013. The *Autographa californica* multiple nucleopolyhedrovirus ORF78 is essential for  
1123 budded virus production and general occlusion body formation. *J Virol* **87**:8441-8450.
- 1124 51. **Tao XY, Choi JY, Kim WJ, An SB, Liu Q, Kim SE, Lee SH, Kim JH, Woo SD, Jin BR, Je**  
1125 **YH.** 2015. *Autographa californica* multiple nucleopolyhedrovirus ORF11 is essential for  
1126 budded-virus production and occlusion-derived-virus envelopment. *J Virol* **89**:373-383.
- 1127 52. **Olszewski J, Miller LK.** 1997. A role for Baculovirus GP41 in budded virus production.  
1128 *Virology* **233**:292-301.
- 1129 53. **Dickison VL, Willis LG, Sokal NR, Theilmann DA.** 2012. Deletion of AcMNPV ac146  
1130 eliminates the production of budded virus. *Virology* **431**:29-39.
- 1131 54. **Hu ZY, Yuan MJ, Wu WB, Liu C, Yang K, Pang Y.** 2010. *Autographa californica* multiple  
1132 nucleopolyhedrovirus ac76 is involved in intranuclear microvesicle formation. *J Virol*  
1133 **84**:7437-7447.
- 1134 55. **McCarthy CB, Dai XJ, Donly C, Theilmann DA.** 2008. *Autographa californica* multiple  
1135 nucleopolyhedrovirus ac142, a core gene that is essential for BV production and ODV  
1136 envelopment. *Virology* **372**:325-339.
- 1137 56. **Yuan MJ, Huang ZQ, Wei DH, Hu ZY, Yang K, Pang Y.** 2011. Identification of *Autographa*  
1138 *californica* nucleopolyhedrovirus ac93 as a core gene and its requirement for intranuclear  
1139 microvesicle formation and nuclear egress of nucleocapsids. *J Virol* **85**:11664-11674.
- 1140 57. **Yuan MJ, Wu WB, Liu C, Wang YJ, Hu ZY, Yang K, Pang Y.** 2008. A highly conserved  
1141 baculovirus gene p48 (ac103) is essential for BV production and ODV envelopment. *Virology*  
1142 **379**:87-96.
- 1143 58. **Peng K, Wu M, Deng F, Song J, Dong C, Wang H, Hu Z.** 2010. Identification of  
1144 protein-protein interactions of the occlusion-derived virus-associated proteins of *Helicoverpa*  
1145 *armigera* nucleopolyhedrovirus. *J Gen Virol* **91**:659-670.
- 1146 59. **Hou DH, Zhang LK, Deng F, Fang W, Wang RR, Liu XJ, Guo L, Rayner S, Chen XW,**  
1147 **Wang HL, Hu ZH.** 2013. Comparative proteomics reveal fundamental structural and  
1148 functional differences between the two progeny phenotypes of a baculovirus. *J Virol*  
1149 **87**:829-839.
- 1150 60. **Xue J, Qiao N, Zhang W, Cheng RL, Zhang XQ, Bao YY, Xu YP, Gu LZ, Han JD, Zhang**  
1151 **CX.** 2012. Dynamic interactions between *Bombyx mori* nucleopolyhedrovirus and its host  
1152 cells revealed by transcriptome analysis. *J Virol* **86**:7345-7359.
- 1153 61. **Salem TZ, Zhang F, Xie Y, Thiem SM.** 2011. Comprehensive analysis of host gene  
1154 expression in *Autographa californica* nucleopolyhedrovirus-infected *Spodoptera frugiperda*  
1155 cells. *Virology* **412**:167-178.
- 1156 62. **Granados RR, Lawler KA.** 1981. In vivo pathway of *Autographa californica* baculovirus  
1157 invasion and infection. *Virology* **108**:297-308.
- 1158 63. **Volkman LE, Goldsmith PA.** 1985. Mechanism of neutralization of budded *Autographa*  
1159 *californica* nuclear polyhedrosis virus by a monoclonal antibody: Inhibition of entry by  
1160 adsorptive endocytosis. *Virology* **143**:185-195.

- 1161 64. **Hefferon KL, Oomens AG, Monsma SA, Finnerty CM, Blissard GW.** 1999. Host cell  
1162 receptor binding by baculovirus GP64 and kinetics of virion entry. *Virology* **258**:455-468.
- 1163 65. **Fang MG, Nie YC, Theilmann DA.** 2009. AcMNPV EXON0 (AC141) which is required for  
1164 the efficient egress of budded virus nucleocapsids interacts with beta-tubulin. *Virology*  
1165 **385**:496-504.
- 1166 66. **Biswas S, Blissard GW, Theilmann DA.** 2016. *Trichoplusia ni* kinesin-1 associates with  
1167 *Autographa californica* multiple nucleopolyhedrovirus nucleocapsid proteins and is required  
1168 for production of budded virus. *J Virol* **90**:3480-3495.
- 1169 67. **Baur T, Ramadan K, Schlundt A, Kartenbeck J, Meyer HH.** 2007. NSF- and  
1170 SNARE-mediated membrane fusion is required for nuclear envelope formation and  
1171 completion of nuclear pore complex assembly in *Xenopus laevis* egg extracts. *J Cell Sci*  
1172 **120**:2895-2903.
- 1173 68. **Li SN, Wang JY, Yuan MJ, Yang K.** 2014. Disruption of the baculovirus core gene *ac78*  
1174 results in decreased production of multiple nucleocapsid-enveloped occlusion-derived virions  
1175 and the failure of primary infection in vivo. *Virus Res* **191**:70-82.  
1176

1177 **Figure legends**

1178 **Figure 1**

1179 **Expression profiles of the components of the cellular SNARE system**  
1180 **before and during AcMNPV infection.** Transcription data for SNARE system  
1181 components were retrieved from a transcriptome analysis of AcMNPV infected  
1182 Tnms42 cells (33) and are grouped into panels A-F according to the SNARE  
1183 genes that are involved in a specific pathway or complex. Measurements of  
1184 transcript levels (RPKM, reads per kilobase per million reads) from samples  
1185 from control (C, uninfected) or infected cells at various time points post  
1186 infection (h p.i., hours post infection) are plotted. The RPKM values (total  
1187 RPKM<5) for  $\gamma$ -SNAP and Syx17 were cutoff in the transcriptome analysis (33).  
1188 The ortholog of Syx4 was not found in the transcriptome database. Error bars  
1189 represent standard deviations from the mean of three replicates. Host gene  
1190 abbreviations are detailed in the legend to Table 3.

1191 **Figure 2**

1192 **Transcript levels of NSF in AcMNPV-infected Sf9 cells.** Sf9 cells were  
1193 infected with wild-type AcMNPV at an MOI of 10 and total RNAs were isolated  
1194 from uninfected (C, control) cells or infected cells at various time points post  
1195 infection (1-48 h p.i.) and transcribed into cDNA. Transcript levels of NSF were  
1196 measured by quantitative real-time PCR. Error bars represent standard  
1197 deviations from the mean of three replicates. h p.i., hours post infection.

1198 **Figure 3**

1199 **Transient expression of GFP-tagged wild-type (WT) and dominant**  
1200 **negative (DN) NSF proteins in Sf9 cells.** (A) Schematic representation of  
1201 domain structure and GFP fusions of WT and DN NSF constructs (NSF-GFP,

1202 NSF<sup>E329Q</sup>-GFP, NSF<sup>R385A</sup>-GFP). NSF domains are abbreviated as: N, NSF-N  
1203 domain; D1, the first ATP-binding domain; D2, the second ATP-binding domain.  
1204 (B) Western blot analysis of GFP-tagged NSF proteins transiently expressed in  
1205 Sf9 cells. GFP and NSF-GFP fusions were detected with an anti-GFP  
1206 polyclonal antibody. The anti- $\beta$ -actin blot served as a loading control. (C)  
1207 Subcellular localization of WT and DN NSF-GFP fusion proteins in transfected  
1208 cells by epifluorescence microscopy (left panels, Epi) and confocal microscopy  
1209 (right panels, Confocal). (D) Viability of transfected cells expressing WT or DN  
1210 NSF proteins was measured at various times post-transfection (12-36 h) using  
1211 a tetrazolium-based cell viability assay as described in the Materials and  
1212 Methods section. Error bars represent standard deviations from the mean of  
1213 three replicates.

1214 **Figure 4**

1215 **Effects of DN NSF expression (A, B) and NSF knock-down (C, D) on**  
1216 **AcMNPV production.** (A, B) Sf9 cells were co-transfected with two plasmids  
1217 expressing a) GP64 and b) either WT NSF (NSF-GFP), DN NSF  
1218 (NSF<sup>E329Q</sup>-GFP or NSF<sup>R385A</sup>-GFP), or GFP. At 12 h p.t., cells were infected with  
1219 the *gp64*-knockout virus (mCherryGUS-*gp64*<sup>ko</sup>) at an MOI of 1 or 5. At 24 h p.i.,  
1220 expression of GP64 and GFP-tagged WT and DN NSF in transfected-infected  
1221 cells was confirmed by Western blot analysis of cell lysates (A). Effects of DN  
1222 NSF proteins were analyzed by measurements the titers of infectious BV  
1223 released from transfected-infected cells (B). (C) Sf9 cells were transfected with  
1224 a NSF-MycpBlue plasmid or co-transfected with a NSF-MycpBlue plasmid and  
1225 the dsRNA targeting NSF or GFP (dsNSF, dsGFP). At 24 and 48 h p.t., the  
1226 transfected cells were collected and the expression of Myc-tagged NSF was



1227 detected by Western blot with an anti-Myc polyclonal antibody. The anti- $\beta$ -actin  
1228 blot served as a loading control. (D) Sf9 cells were mock transfected (Mock) or  
1229 transfected with the dsRNA targeting NSF or GFP (dsNSF, dsGFP). At 48 h p.t.,  
1230 the transfected cells were infected with wild-type AcMNPV at an MOI of 5. At  
1231 24 h p.i., the cell culture supernatants were collected and the virus titers were  
1232 determined by TCID<sub>50</sub> assays. Error bars represent standard deviations from  
1233 the mean of three replicates. \*\*\*,  $p < 0.0005$ ; \*\*\*\*,  $p < 0.00005$  (by unpaired  $t$   
1234 test).

### 1235 **Figure 5**

1236 **Effects of DN NSF on early stages of AcMNPV infection.** The effects of DN  
1237 NSF proteins on early and late viral gene expression and viral DNA replication  
1238 were examined. Sf9 cells were co-transfected with two plasmids expressing a)  
1239 GP64 and b) either WT NSF (NSF-GFP) or DN NSF (NSF<sup>E329Q</sup>-GFP or  
1240 NSF<sup>R385A</sup>-GFP), or GFP. At 12 h p.t., the transfected cells were infected with a  
1241 *gp64*-knockout virus (LacZGUS-*gp64*<sup>ko</sup>). Early gene expression was monitored  
1242 by analyzing AcMNPV *ie1* early/late promoter driven  $\beta$ -Gal activity at 6 h p.i.  
1243 (A). Late phase gene expression was monitored by analyzing AcMNPV *p6.9*  
1244 late promoter driven GUS activity at 24 h p.i. (B). Viral DNA replication was  
1245 monitored by quantitatively real-time PCR analysis of viral genomic DNA  
1246 extracted from transfected-infected cells at 24 h p.i. (C). Error bars represent  
1247 standard deviations from the mean of three replicates. \*\*,  $p < 0.005$ ; \*\*\*,  
1248  $p < 0.0005$  (by unpaired  $t$  test).

### 1249 **Figure 6**

1250 **Effects of DN NSF on AcMNPV entry.** Sf9 cells were transfected with  
1251 plasmids expressing either WT NSF (NSF-GFP), DN NSF (NSF<sup>E329Q</sup>-GFP or

1252 NSF<sup>R385A</sup>-GFP), or GFP. At 12 h p.t., the cells were infected at 4° for 60 min  
1253 with an AcMNPV virus containing mCherry-tagged VP39 capsid protein. After  
1254 raising the culture temperature to 27° for 60 min, the internalization and  
1255 transport of entering virions were analyzed by quantitative real-time PCR  
1256 analysis of viral DNA from cell lysates (A) and by confocal microscopic  
1257 detection of mCherry-tagged capsids (B). Error bars represent standard  
1258 deviations from the mean of three replicates. Scale bar, 10 µm; \*, p<0.05 (by  
1259 unpaired *t* test).

### 1260 **Figure 7**

#### 1261 **Effects of DN NSF proteins on production of infectious budded virions.**

1262 Sf9 cells were transfected with bacmid DNA expressing either WT NSF  
1263 (NSF-GFP), DN NSF (NSF<sup>E329Q</sup>-GFP or NSF<sup>R385A</sup>-GFP), or GFP. Transfection  
1264 activity was monitored by analysis of GFP-positive cells (A). Percentages of  
1265 GFP positive cells at 24 h p.t. are indicated below each micrograph of GFP  
1266 epifluorescence. Late phase gene expression was monitored by analysis of  
1267 GUS activity from a *p6.9* late promoter driven GUS gene at 24 h p.t. (B).  
1268 Production of infectious BV was measured by TCID<sub>50</sub> assay of cell culture  
1269 supernatants collected at 24 h p.t. (C). Error bars represent the standard  
1270 deviations from the mean of three replicates.

### 1271 **Figure 8**

1272 **Effects of DN NSF on cell surface levels of GP64.** Sf9 cells were transfected  
1273 with 2.5 µg bacmid DNA expressing GFP-tagged NSF proteins (WT or DN) or  
1274 GFP. To generate a standard curve for GP64 surface levels and for cell-cell  
1275 fusion analysis, cells were transfected with 0.5-2.5 µg bacmid DNA expressing  
1276 GFP-tagged WT NSF. At 24 h p.t., the expression, cell-surface localization,

1277 and fusion activity of GP64, and infectious virus production were analyzed. (A)  
1278 Western blot analysis of the expression and oligomerization of GP64 on  
1279 reducing (R) and non-reducing (NR) gels. The anti- $\beta$ -actin blot served as a  
1280 loading control. (B, C) The transfected cells were fixed and the cell surface  
1281 localization of GP64 was detected by cELISA using AcV5 antibody (B), or by  
1282 indirect immunofluorescence using AcV1 antibody (C). (D) Transfected cells  
1283 were treated with PBS at pH 5.0 to induce GP64-mediated cell-cell syncytium  
1284 formation. The percentages of nuclei in syncytia (defined as more than five  
1285 nuclei per syncytium) in five fields was calculated. (E) Infectious BV production  
1286 from transfected cells expressing WT or DN NSF proteins, or GFP was  
1287 determined by TCID50 assays. Error bars represent the standard deviations  
1288 from the mean of three replicates. \*,  $p < 0.05$ ; \*\*,  $p < 0.005$  (by unpaired *t* test).

1289 **Figure 9**

1290 **TEM analysis of AcMNPV-infected Sf9 cells expressing WT or DN NSF**  
1291 **proteins.** Sf9 cells were transfected with AcMNPV bacmids expressing either  
1292 wild-type NSF (A-D), or dominant negative NSF proteins NSF<sup>E329Q</sup>-GFP (E-H)  
1293 or NSF<sup>R385A</sup>-GFP (I-L). At 48 h post-transfection, the bacmid-transfected cells  
1294 were fixed and analyzed by transmission electronic microscopy.  
1295 Electron-dense virogenic stroma (VS) and intranuclear microvesicles (IM) were  
1296 observed in cells expressing both WT NSF and DN NSF (A vs. E or I). White  
1297 and black triangles show intranuclear microvesicles (IM) and nucleocapsids  
1298 associated with the membranous vesicular structures, respectively (Panels B  
1299 vs. F vs. J). Progeny nucleocapsids (white arrows) appear to be budding into  
1300 the nuclear membrane (NM, black arrows) (C) and free in the cytoplasm (D) in  
1301 cells expressing WT NSF. In contrast, nucleocapsids (white arrows) were

1302 found primarily in large perinuclear space or vesicular structures (black  
1303 triangles) associated with the nuclear membrane in cells expressing DN NSF  
1304 (G, H, K, and L). Plasma membrane (PM); Scale bar, 500 nm.

1305 **Figure 10**

1306 **Co-immunoprecipitation analysis of NSF and AcMNPV proteins.** Sf9 cells  
1307 were transfected or co-transfected with two plasmids separately expressing  
1308 NSF-Myc and a HA-tagged viral protein. At 36 h p.t., the cells were lysed and  
1309 the proteins were immunoprecipitated with anti-HA monoclonal antibody and  
1310 protein-G agarose. The precipitates (Co-IP) were detected on Western blots  
1311 with an anti-Myc polyclonal antibody (right panel in each group). The cell  
1312 lysates (Lysate Input) were also examined on Western blots with an anti-HA  
1313 monoclonal antibody (Lysate Input, top panels) or an anti-Myc polyclonal  
1314 antibody (Lysate Input, bottom panels).

1315 **Figure 11**

1316 **BiFC analysis of NSF and AcMNPV protein associations.** Sf9 cells were  
1317 co-transfected with a pair of BiFC plasmids: one expressing NSF-HA-Nm  
1318 (NSF-Nm) and the other expressing a viral protein fused with Myc-Cm  
1319 (Ac#-Cm or Cm-Ac146). As controls, cells were transfected with plasmid pairs  
1320 expressing GP41-HA-Nm and GP41-Myc-Cm, or GP41-HA-Nm and  
1321 Lef3-Myc-Cm. At 36 h p.t., cells were examined for fluorescence  
1322 complementation by epifluorescence microscopy (A) and the percentage of  
1323 mCherry-positive cells in five fields was calculated (B). The expression of each  
1324 construct in co-transfected cells was confirmed by Western blot analysis with  
1325 anti-Myc antibody (A, panels a) or anti-HA antibody (A, panels b). Error bars  
1326 represent the standard deviations from the mean of three replicates. \*,  $p < 0.05$ ;

1327 \*\*,  $p < 0.005$ ; \*\*\*\*,  $p < 0.00005$  (by unpaired *t* test).

1328 **Figure 12**

1329 **Detection of NSF in budded virions of AcMNPV.** Sf9 cells were transfected  
1330 with bacmid NSF-MycBac, which expresses a Myc-tagged WT NSF protein. At  
1331 72 h p.t., cell supernatants were collected and the budded virions were purified  
1332 by sucrose density gradient centrifugation. The transfected cells and the  
1333 purified virions were analyzed on Western blots using anti-GP64, anti-VP39,  
1334 anti-Myc, and anti-GUS antibodies. BV, budded virions. Typical and long (left  
1335 and right, respectively) exposures of Western blots are shown, illustrating the  
1336 presence of NSF at low quantities in BV preparations.

1337 **Figure 13**

1338 **A hypothetical model for the role of cellular NSF protein in the infection**  
1339 **cycle of AcMNPV.** Steps at which NSF is potentially required for trafficking  
1340 during budded virion entry and progeny nucleocapsid egress are indicated as  
1341 dashed lines. BV, budded virions; CCV, clathrin-coated vesicles; EE, early  
1342 endosome; ER, endoplasmic reticulum; LE, late endosome; MVB,  
1343 multivesicular bodies; NC, nucleocapsid; NPC, nuclear pore complex; NSF,  
1344 N-ethylmaleimide-sensitive factor; VS, virogenic stroma.

**Table 1.** PCR primers

Primer	Sequence (5' to 3')	Description
SfNsfF	atgtctgcaatgCGGATGAAG	Amplification of the ORF of Sf9 NSF
SfNsfR	ttattgtacattGGTGCCTAGGTC	
SfNsfXF	aattctagaatgTCTGCAATCGGATGAAG	Amplification of the ORF of Sf9 NSF
SfNsfER	aatgaattctgattGTACATTGGTGCCTAGGTC	
NsfF	accgccttagccgctgaact	Amplification of 90 bp of Sf9 NSF
NsfR	agactccgTGAATCCGACCATGT	
E329QF	cagatcgacgctattTGCaaagc	Construction of E329Q and R385A mutants
E329QR	gcaaatagcgctgactGGTCAAAGATGATAATGTGGA	
R385AF	gtcccggctgctcGAGGTTc	
R385AR	ctcgagacgaccgggagccatcaacgcctcgtcaatcat	
HANmF	aatgaattcaccatacagatgttccagattacgctgggacgtcggggtggaag	Construction of HA-NmpBlue
	cggtatggTGAAGCGGCGGAGGA	
NmFt	cgagcggatgtaacccgaggactaaatgaataataaaaattgtatca	Construction of Myc-CmpBlue
NmRt	tgatacaattttattattacatttagtctcgggtacatccgctcg	
64pAR	attaagcttcacactcgctattTGAACAT	
MycCmF	aatgaattcgaacaaaactcatctcagaagaggatctggggacgtcgggT	
	ggaagcggTGGCGCCCTGAAGGGCGAGATC	
CmFt	cggcatggacgagctgtacaagtagatgaataataaaaattgtatca	Construction of Cm-MycpBlue
CmRt	tgatacaattttattattacactactgtacagctcgtccatgccg	
64pAR	attaagcttcacactcgctattTGAACAT	
NmHAF	aattctagaatggTGAAGGGCGAGGAG	
NmHAR	attggatccagcgaatctggaacatcgtatgggtaaccgctccaccgcgac	
	tcccgtcctcgggTACATCCGCTCG	
CmMycF	aattctagaatgggCGCCCTGAAGGGCGAGATC	Construction of Cm-MycpBlue
CmMycR	aatggatccagatcctctctgagatgagttttgtcaccgctccaccgcgac	
	gtcccctgtacagctcgtccatgccg	
nMycF	ctagaatggaacaaaactcatctcagaagaggatctgaatg	Construction of pIE-Myc-MCS
nMycR	gatccattcagatcctctctgagatgagttttgtccatt	
nHaF	ctagaatgtaccatacagatgtccagattacgctg	Construction of pIE-HA-MCS
nHaR	gatccagcgaatctggaacatcgtatgggtacatt	
cMycF	ataagaattcgaacaaaactcatctcagaagaggatctgaattagatgtaa	Construction of pIE-MCS-Myc
	taataaaaattgtatca	
64pAR	attaagcttcacactcgctattTGAACAT	
cHAF	ataagaattcaccatacagatgtccagattacgcttagatgaataataaaa	Construction of pIE-MCS-HA
	attgtatca	
64pAR	attaagcttcacactcgctattTGAACAT	
NSFiF	ggatcctaatacagactcactatagggactcgcagccctaacaaga	Amplification of the dsDNA of Sf9 NSF
NSFiR	ggatcctaatacagactcactatagggcttagtagcccttgctg	
GFPIF	ggatcctaatacagactcactataggcgtaaacggccacaagttc	Amplification of the dsDNA of GFP
GFPIR	ggatcctaatacagactcactatagggttctcgtgtagtggtcg	

**Table 2.** Plasmids constructed in this study

<b>Purpose</b>	<b>Construct name</b>	
Expression and subcellular localization of NSF and its mutants	NSF-GFPpBlue	
	E329Q-GFPpBlue	
	R385A-GFPpBlue	
Real-time PCR	NSF90pMD18	
Co-immunoprecipitation	GP41-MycpBlue	
	Lef3-MycpBlue	
	NSF-MycpBlue	
	Ac11-HApBlue	
	Ac76-HApBlue	
	Ac78-HApBlue	
	GP41-HApBlue	
	Ac93-HApBlue	
	Ac103-HApBlue	
	Ac142-HApBlue	
	HA-Ac146pBlue	
	Bimolecular fluorescence complementation (BiFC) assay	NSF-HA-NmpBlue*
		Ac11-HA-NmpBlue
Ac76-HA-NmpBlue		
Ac78-HA-NmpBlue		
GP41-HA-NmpBlue		
Ac93-HA-NmpBlue		
Ac103-HA-NmpBlue		
Ac142-HA-NmpBlue		
Nm-HA-Ac146pBlue		
NSF-Myc-CmpBlue <sup>§</sup>		
Ac11-Myc-CmpBlue		
Ac76-Myc-CmpBlue		
Ac78-Myc-CmpBlue		
GP41-Myc-CmpBlue		
Ac93-Myc-CmpBlue		
Ac103-Myc-CmpBlue		
Ac142-Myc-CmpBlue		
Lef3-Myc-CmpBlue		
Cm-Myc-Ac146pBlue		

Note: \*Nm and <sup>§</sup>Cm represent the N- and C-terminus of mCherry, respectively.

**Table 3.** The SNARE proteins in yeast, human, and insects

Function sites	Classification	Species			
		Yeast	Human	Insects <sup>§</sup>	
Endosome /Lysosome	Qa	Pep12	Syx7	+	
		Vam3	-	-	
		-	Syx13	-	
		-	Syx17	+ <sup>1</sup>	
	Qb	Vti1	-	Syx20	+ <sup>2</sup>
			Vti1a } Vti1b }		Vti1 <sup>3</sup>
	Qc	Syx8	Syx8	+ <sup>4</sup>	
		Tlg1	Syx6	+	
		-	Syx10	-	
	R	Vam7	-	-	
		Nyv1	VAMP7	+	
		-	Endob/VAMP8	-	
	Endoplasmic reticulum	Qa	Ufe1	Syx18	+
			Sec20	Sec20	+
Qc		Slt1/Use1	Use1	+	
R		Sec22	Sec22a } Sec22b } Sec22c }	Sec22	
		-			
		-			
Golgi apparatus		Qa	Sed5	Syx5	+
			Tlg2	Syx16	+
		Qb	Bos1	Memb	+
			Gos1	Gos28	+
	Qc	Bet1	Bet1	+	
		Sft1	Gos15	-	
	R	Ykt6	Ykt6	+	
	Polarization	R	-	Amisyn	-
-			Tom1 } Tom2 }	Tom	
Sro7/Sro77			Lgl1 } Lgl2 }	Lgl	
-					
-					
Regulatory complex	Sec17	-	α - SNAP	+	
		-	β - SNAP	-	
		-	γ - SNAP	+	
Sec18	NSF	+			
Secretion pathway	Qa	Sso1/Sso2	Syx1a } Syx1b }	Syx1	
		-	Syx2	-	
		-	Syx3	-	
		-	Syx4	+ <sup>6</sup>	
		-	Syx11	-	
		-	Syx19	-	
		Qbc*	Sec9	SNAP-25a } SNAP-25b }	SNAP-25
			SPO20		
	-		SNAP-23	-	
	R	-	SNAP-29	+	
		Snc1/Snc2	SNAP-47	-	
		-	Syb1 } Syb2 } Syb3 }	Syb	
	-	Myob	-		

**Note:** <sup>§</sup>Insects represent sequenced insect genomes, which including those of *Acyrtosiphon pisum*, *Aedes aegypti*, *Anopheles gambiae*, *Apis mellifera*, *Bombyx mori*, *Culex quinquefasciatus*, *Danaus plexippus*, *Drosophila melanogaster*, *Harpegnathos saltator*, *Nasonia vitripennis*, *Pediculus humanus corporis*, *Tribolium castaneum*. \*Qbc represents the SNARE proteins possess one Qb-SNARE motif and one Qc-SNARE motif.



+<sup>1</sup>: absent in *Culex quinquefasciatus*, *Pediculus humanus corporis*;

+<sup>2</sup>: absent in *Acyrtosiphon pisum*;

+<sup>3</sup>: Two orthologs of Vti1 were found in *Acyrtosiphon pisum*, *Anopheles gambiae*, *Apis mellifera*, *Culex quinquefasciatus*, *Drosophila melanogaster*, *Harpegnathos saltator*, *Tribolium castaneum*;

+<sup>4</sup>: absent in *Bombyx mori*, *Danaus plexippus*;

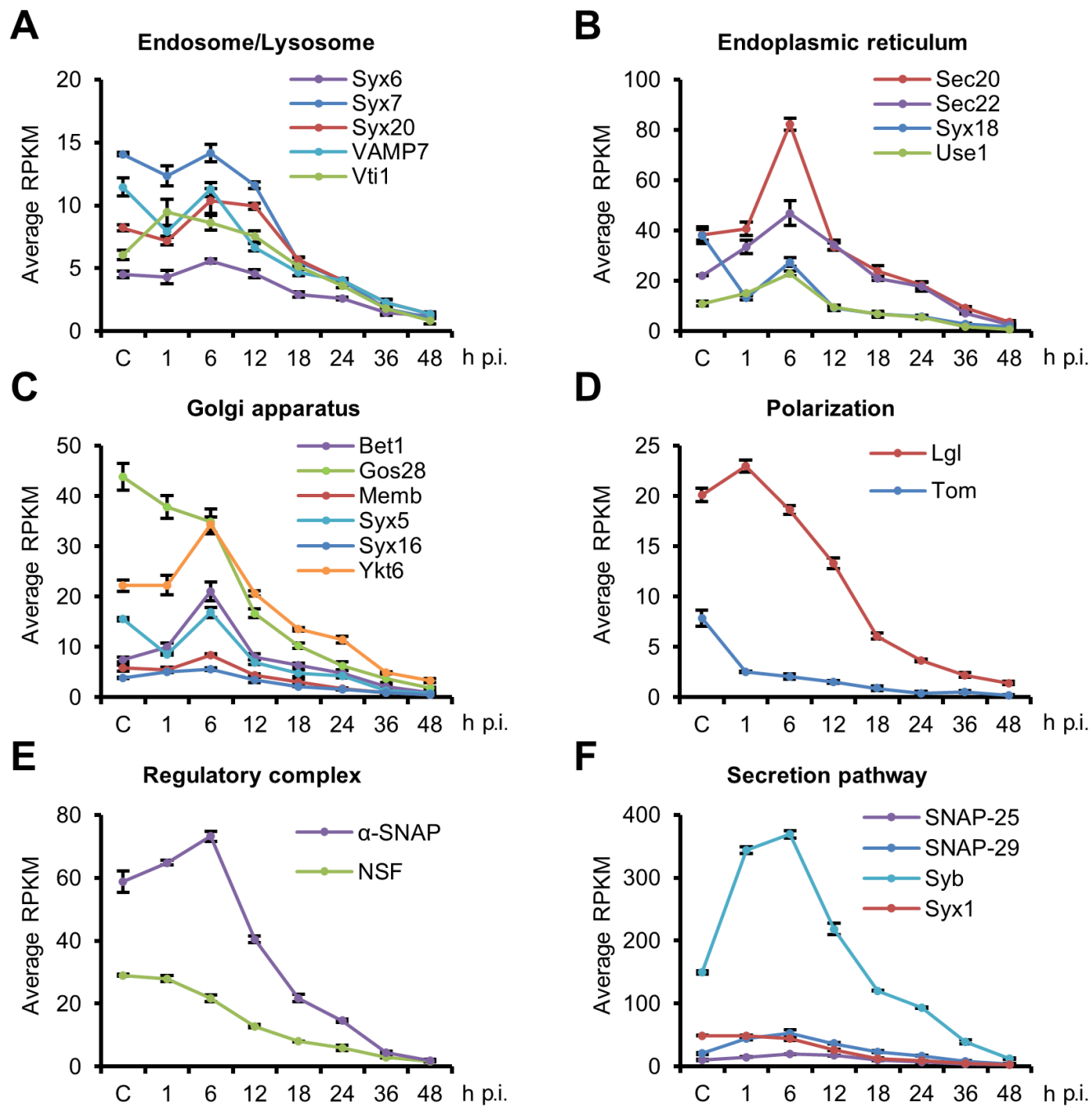
+<sup>5</sup>: only present in *Apis mellifera*, *Nasonia vitripennis*;

+<sup>6</sup>: absent in *Harpegnathos saltator*, *Pediculus humanus corporis*;

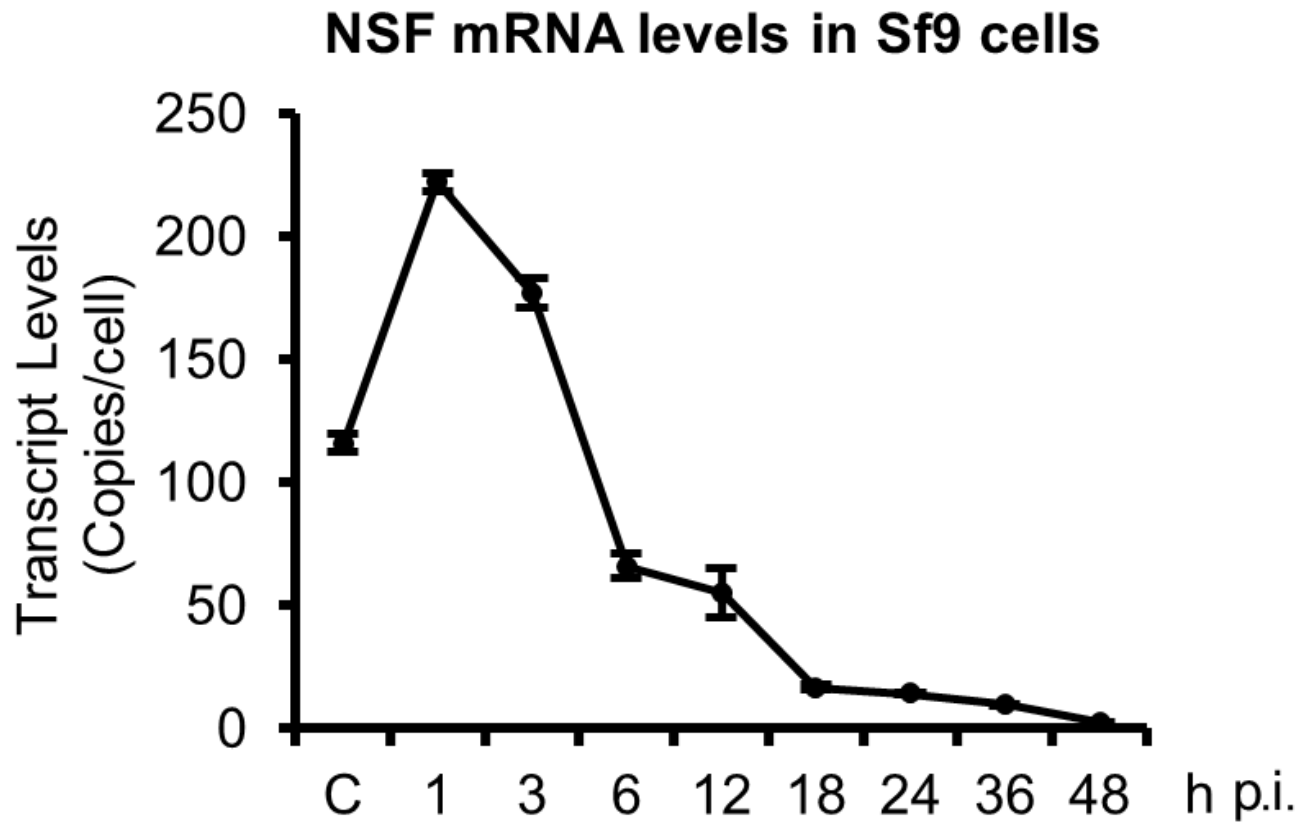
Abbreviations:  $\alpha$ -SNAP,  $\alpha$ -soluble NSF attachment protein; Bet1, blocked early in transport; Bos1, Bet1 suppressor 1; Endob, endobrevin; Gos#, Golgi SNARE protein with a size of # kDa; Lgl#, lethal giant larvae #; Memb, membrin; Myob, myobrevin; NSF, N-ethylmaleimide sensitive factor; Nyv1, new yeast v-SNARE; Pep12, carboxypeptidase Y-deficient; Sec#, secretory mutant # protein; Sed5, suppressor of Erd2 deletion; Stt1, suppressor of Sed5; Sl1, SNARE-like tail-anchored protein 1; Snc1/Snc2, suppressor of the null allele of CAP; SNAP-#, synaptosome-associated protein of # kDa; SPO20, SPOulation 20; Sro7/Sro77, suppressor of Rho3; Sso1/Sso2, supressor of Sec1; Syb#, synaptobrevin #; Syx#, syntaxin #; Tlg, T-snare affecting a late Golgi compartment; Tom, tomosyn; Ufe1, unknown function essential 1; Use1, unconventional SNARE in the ER; Vam#, vacuolar morphogenesis #; VAMP#, vesicle-associated membrane protein #; Vti1, Vps10 interacting protein. Ykt6, YKL196c-encoding protein.

# Figure 1

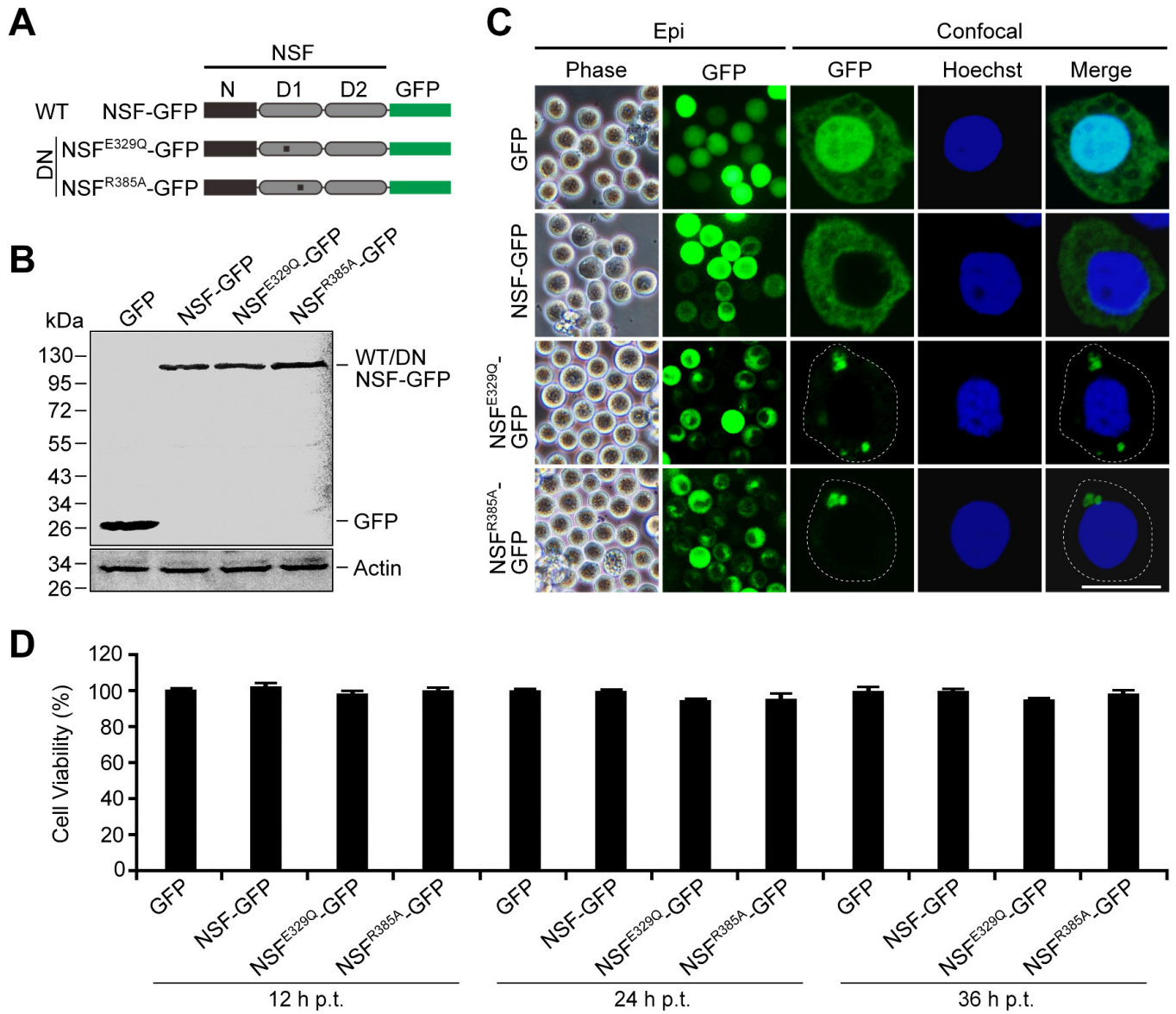
RNA-seq analysis of SNARE mRNAs in AcMNPV-infected *T.ni* cells



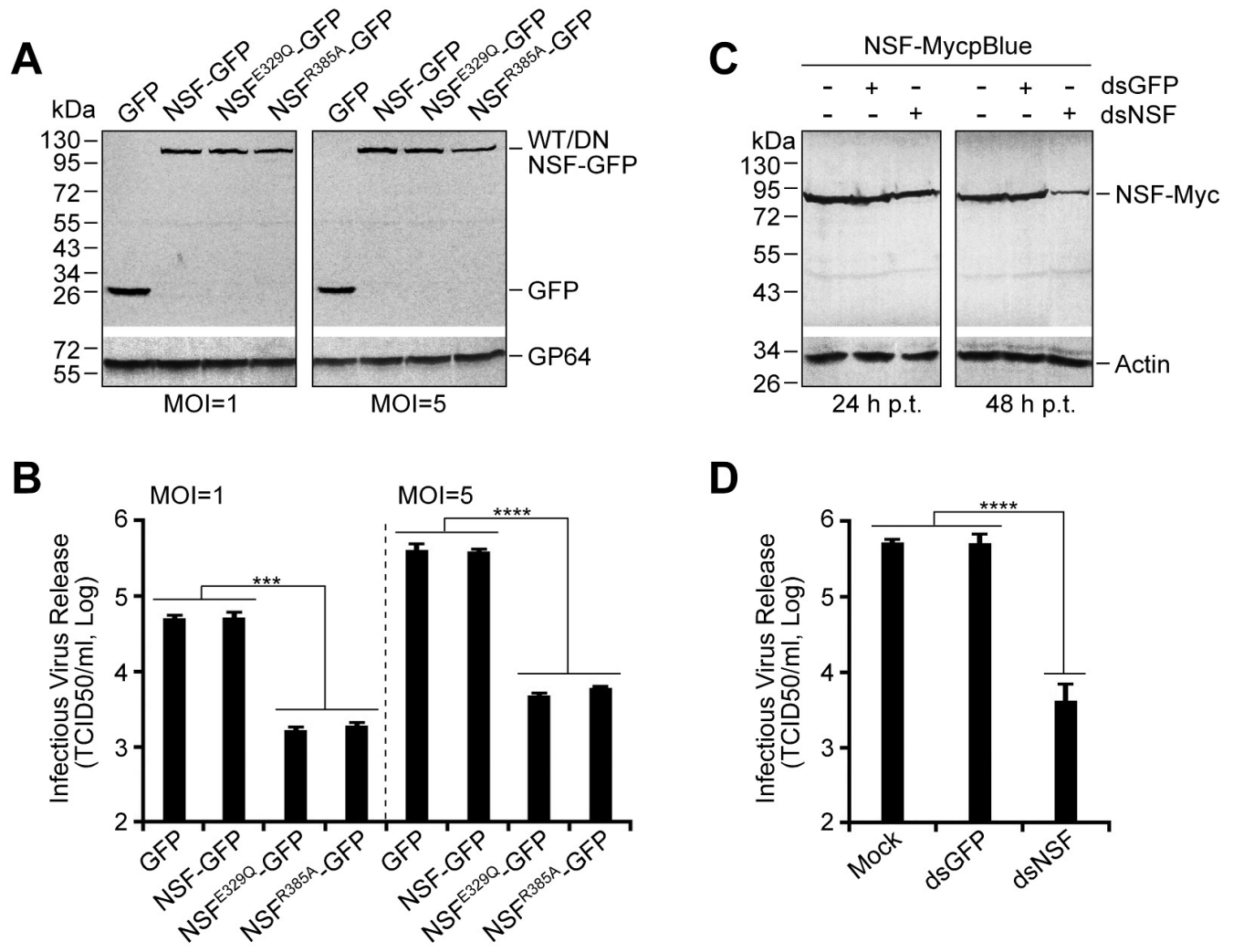
# Figure 2

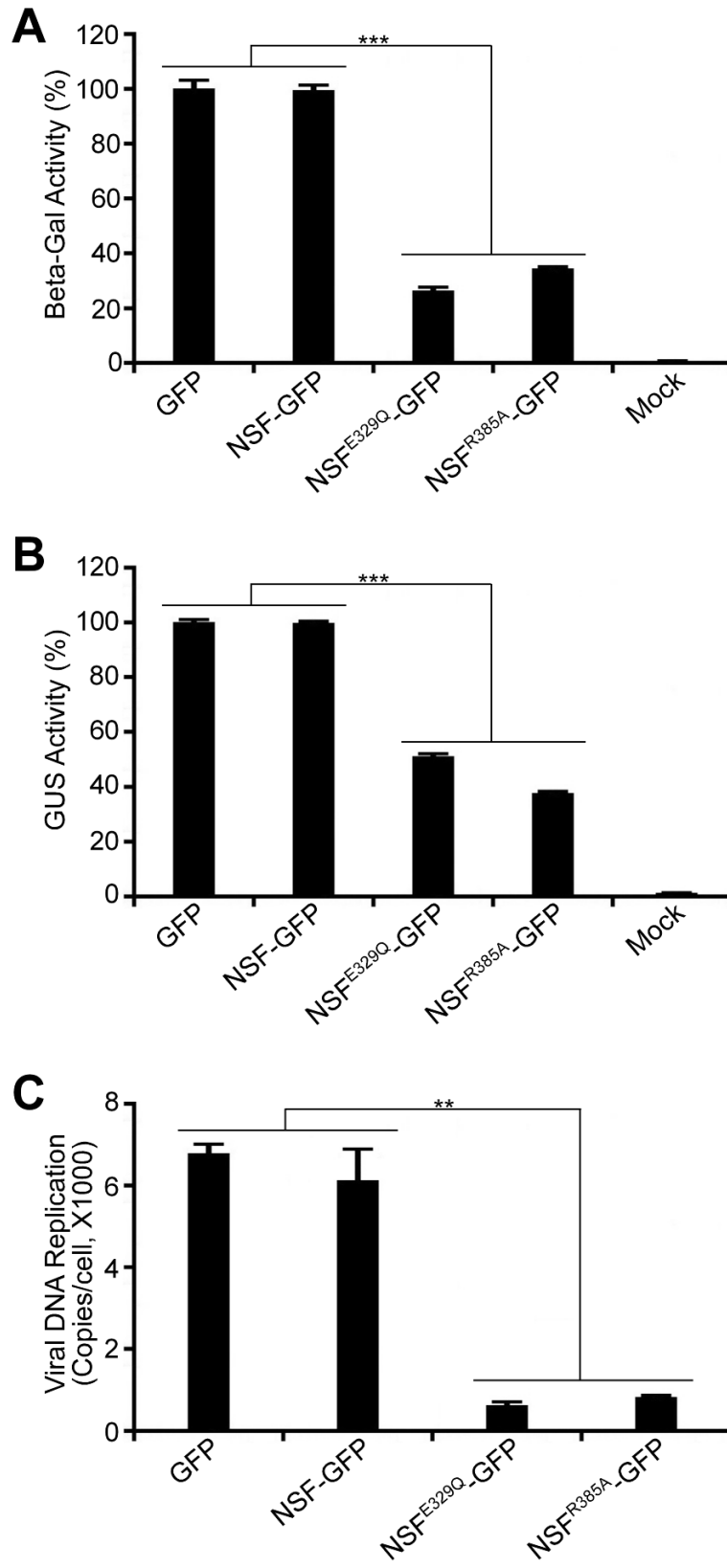


## Figure 3

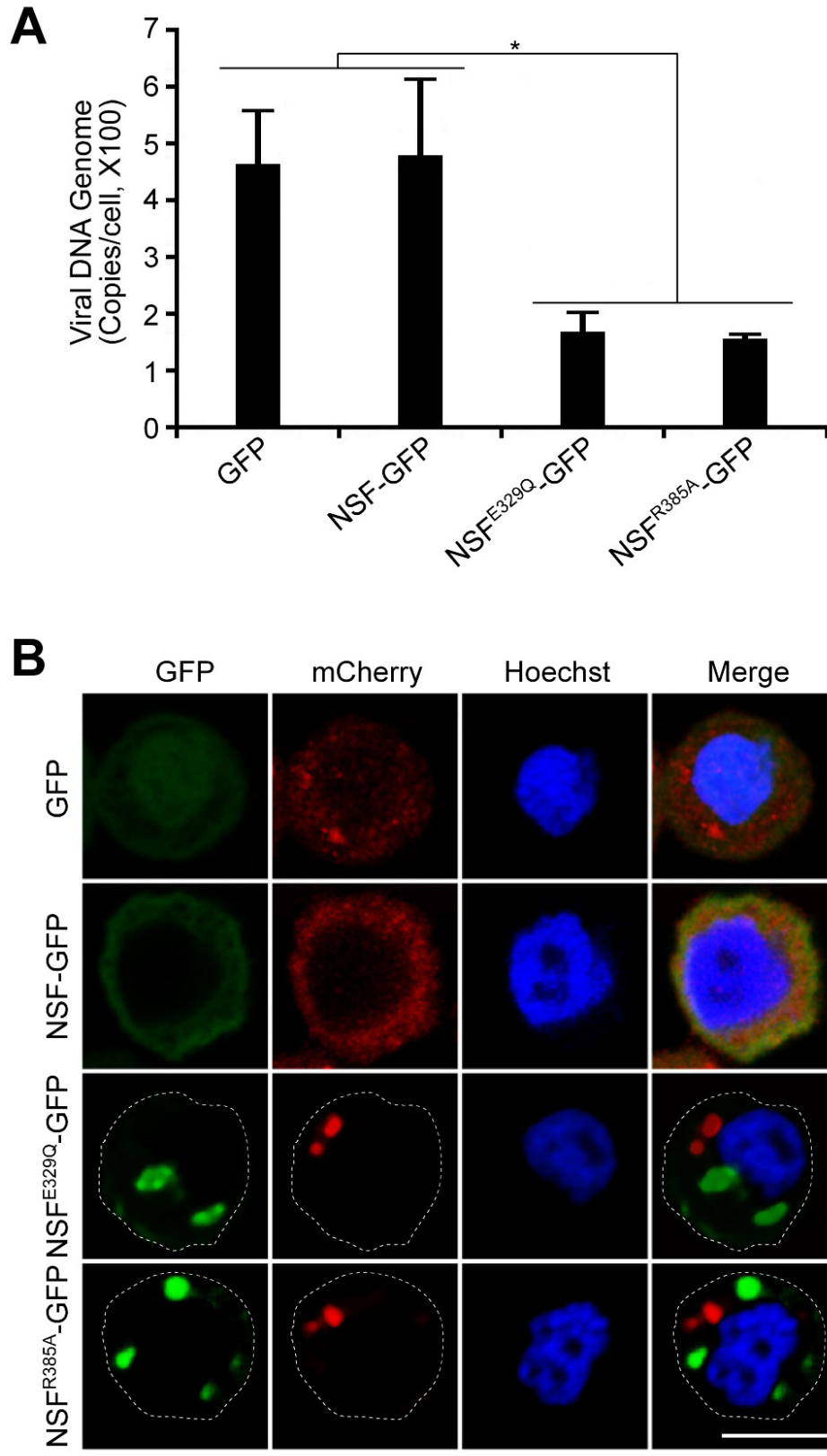


## Figure 4

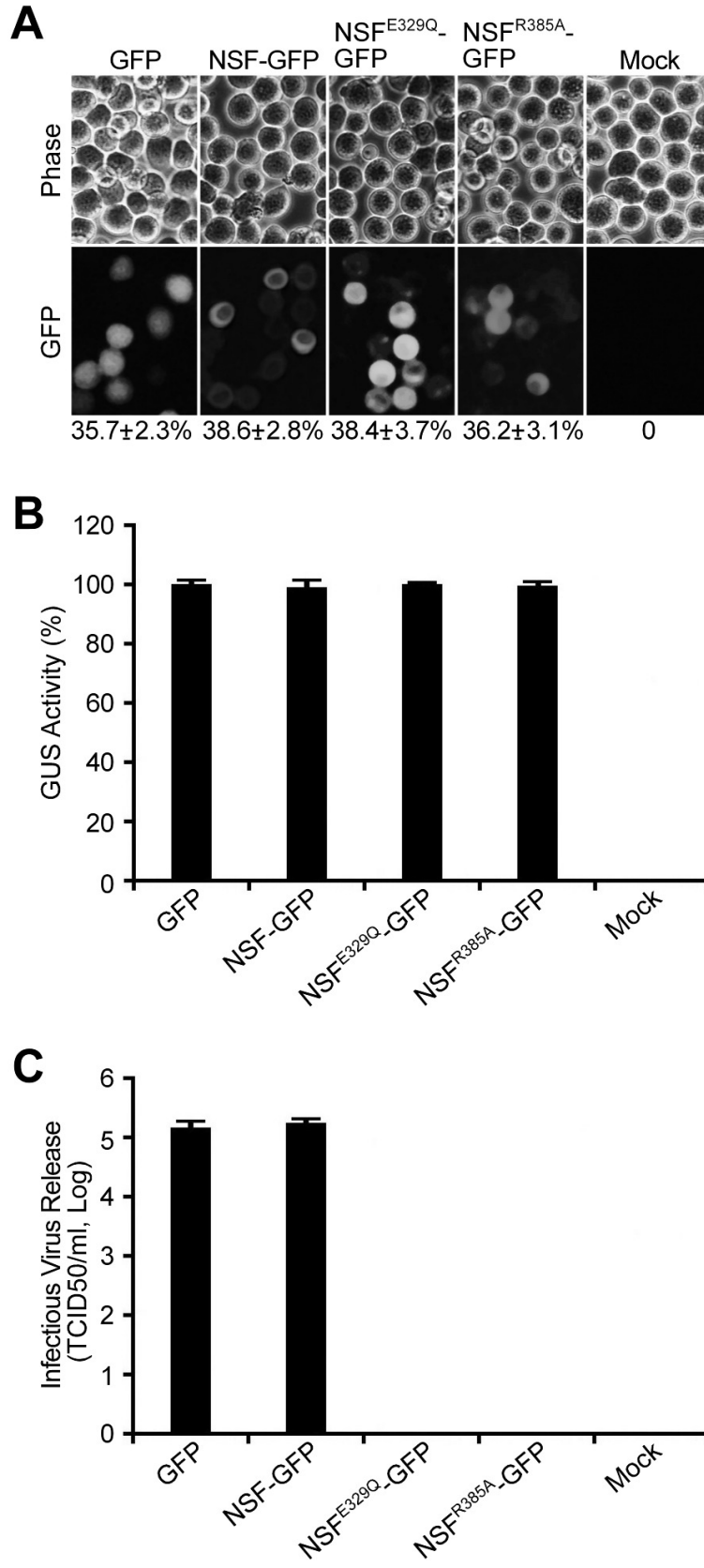


**Figure 5**

## Figure 6

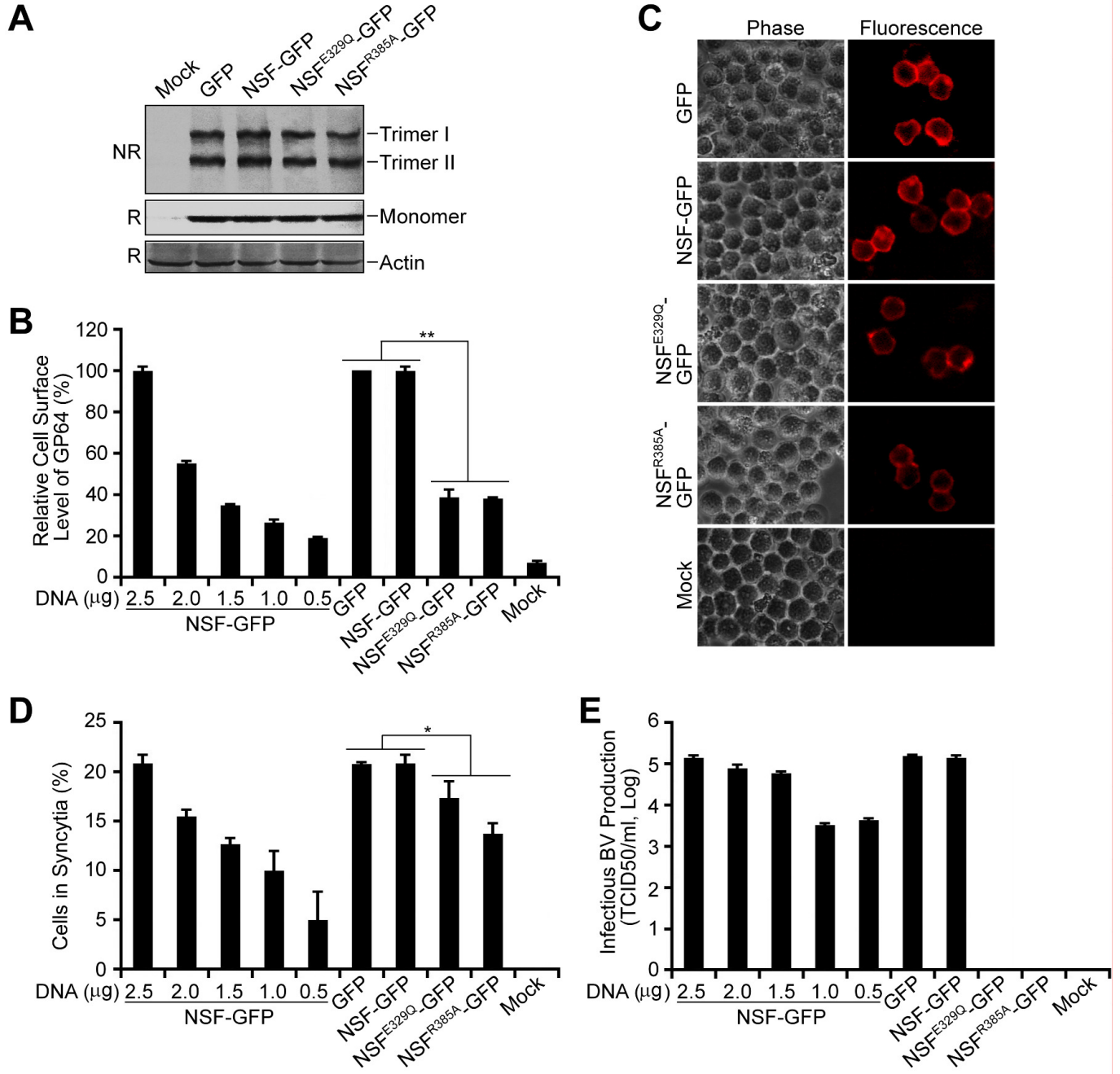


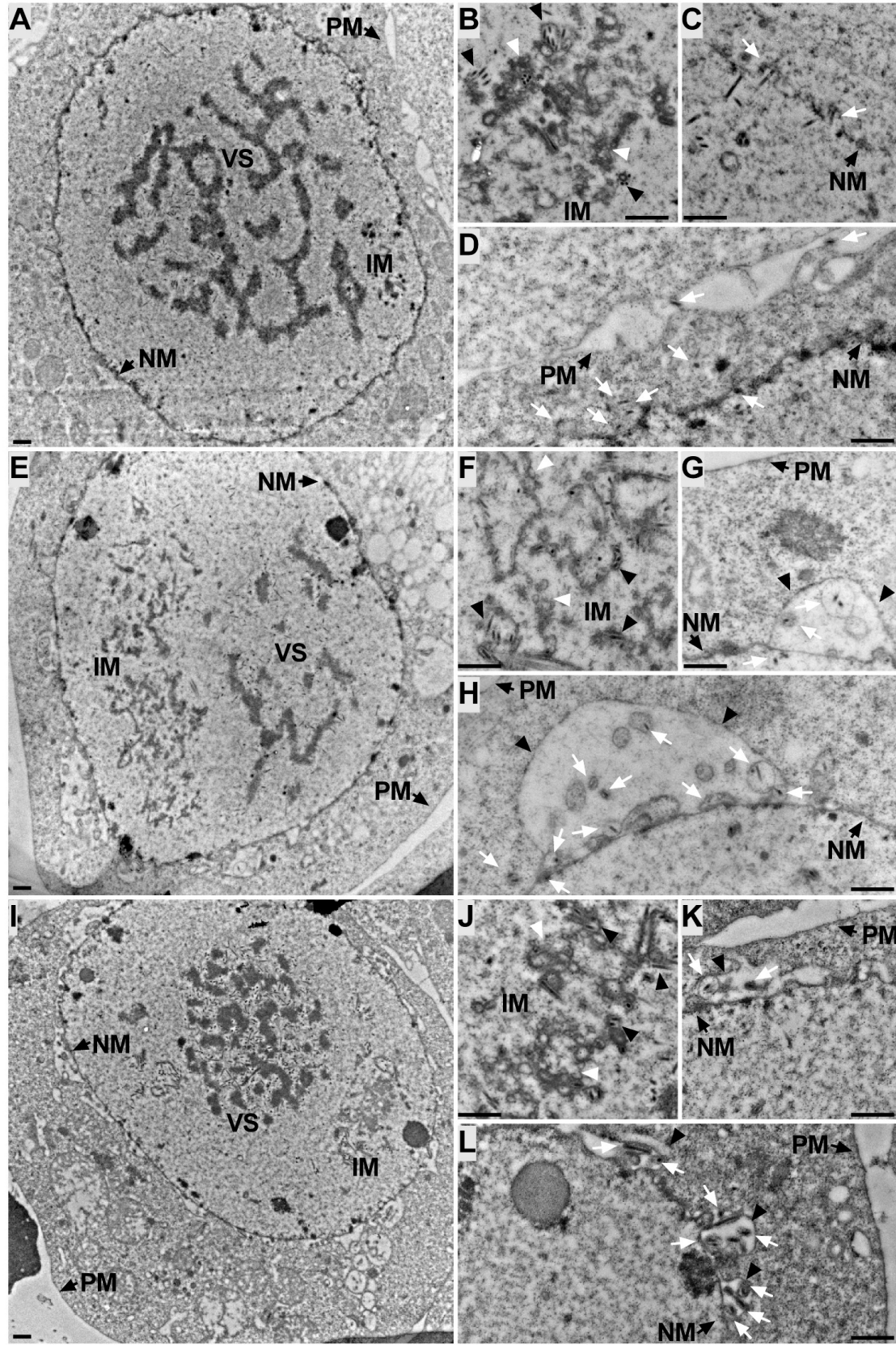
## Figure 7





## Figure 8



**Figure 9**

## Figure 10

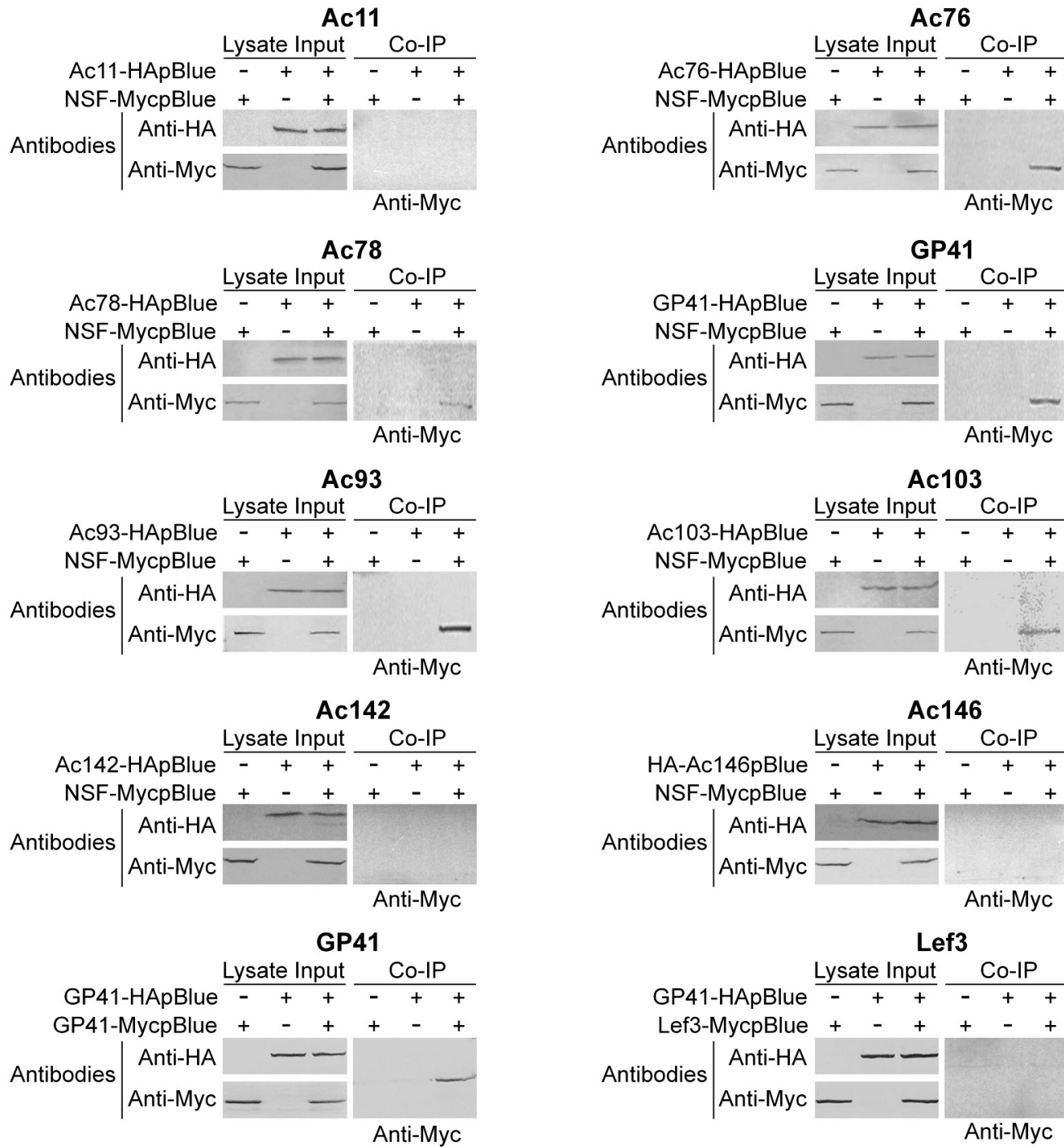


## Figure 11

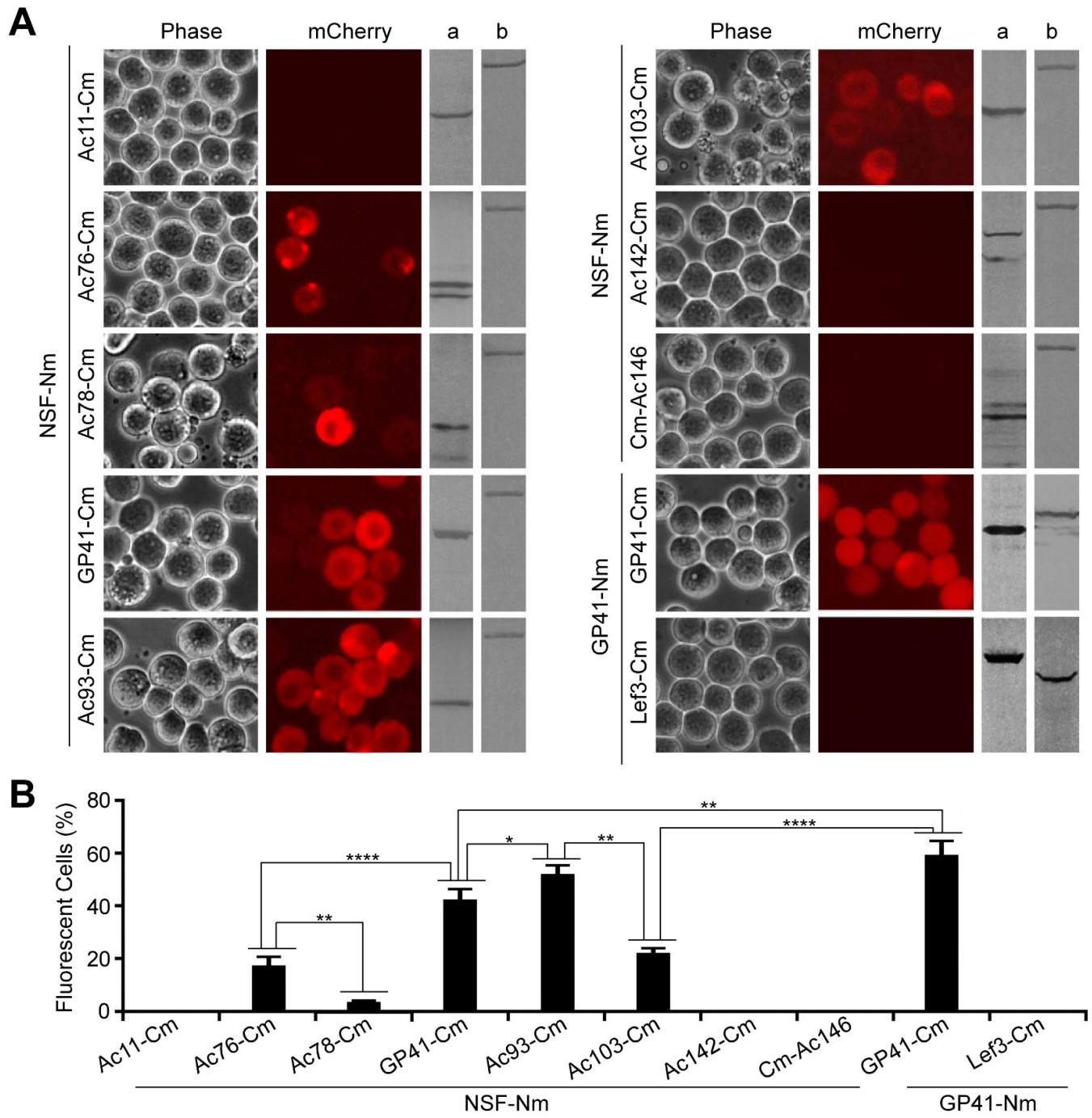


# Figure 12

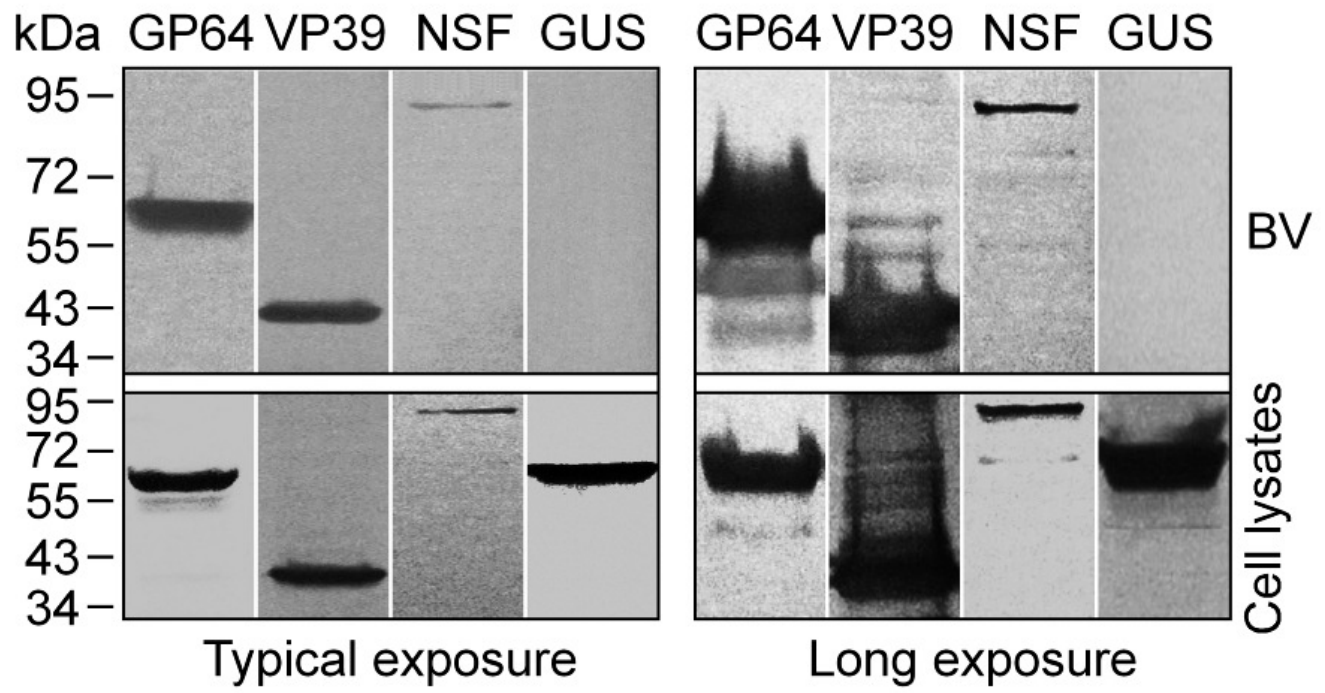


Figure 13

